



Received 13 July 2016

Accepted 9 August 2016

Edited by G. Kostorz, ETH Zurich, Switzerland

Keywords: magnetic structures database; MAGNDATA; commensurate magnetic structures; magnetic space groups; Bilbao Crystallographic Server; magnetic symmetry; irreducible representations.

MAGNDATA: towards a database of magnetic structures. I. The commensurate case

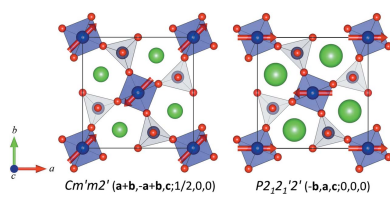
Samuel V. Gallego,^a J. Manuel Perez-Mato,^{a*} Luis Elcoro,^a Emre S. Tasci,^b Robert M. Hanson,^c Koichi Momma,^d Mois I. Aroyo^a and Gotzon Madariaga^a

^aDepartamento de Física de la Materia Condensada, Facultad de Ciencia y Tecnología, Universidad del País Vasco (UPV/EHU), Apartado 644, Bilbao, 48080, Spain, ^bDepartment of Physics Engineering, Hacettepe University, Ankara, 06800, Turkey, ^cDepartment of Chemistry, St Olaf College, Northfield, MN 55057, USA, and ^dNational Museum of Nature and Science, 4-1-1 Amakubo, Tsukuba 305-0005, Japan. *Correspondence e-mail: jm.perez-mato@ehu.es

A free web page under the name *MAGNDATA*, which provides detailed quantitative information on more than 400 published magnetic structures, has been developed and is available at the Bilbao Crystallographic Server (<http://www.crys.t.ehu.es>). It includes both commensurate and incommensurate structures. This first article is devoted to explaining the information available on commensurate magnetic structures. Each magnetic structure is described using magnetic symmetry, *i.e.* a magnetic space group (or Shubnikov group). This ensures a robust and unambiguous description of both atomic positions and magnetic moments within a common unique formalism. A non-standard setting of the magnetic space group is often used in order to keep the origin and unit-cell orientation of the paramagnetic phase, but a description in any desired setting is possible. Domain-related equivalent structures can also be downloaded. For each structure its magnetic point group is given, and the resulting constraints on any macroscopic tensor property of interest can be consulted. Any entry can be retrieved as a magCIF file, a file format under development by the International Union of Crystallography. An online visualization tool using *Jmol* is available, and the latest versions of *VESTA* and *Jmol* support the magCIF format, such that these programs can be used locally for visualization and analysis of any of the entries in the collection. The fact that magnetic structures are often reported without identifying their symmetry and/or with ambiguous information has in many cases forced a reinterpretation and transformation of the published data. Most of the structures in the collection possess a maximal magnetic symmetry within the constraints imposed by the magnetic propagation vector(s). When a lower symmetry is realized, it usually corresponds to an epikernel (isotropy subgroup) of one irreducible representation of the space group of the parent phase. Various examples of the structures present in this collection are discussed.

1. Introduction

The quantitative characterization of the magnetic ordering realized in magnetic phases is an essential part of research into the magnetic properties of solids. It is certainly fundamental for the cross-checking of theoretical models and for the exploration of complex solid-state magnetic phenomena. Furthermore, the determination of magnetic structures, mainly using neutron diffraction data, is a fundamental step in the search for functional materials for magnetic and/or magnetostructural applications. Since the first report of a magnetic structure determined from neutron diffraction data in 1949 (Shull & Smart, 1949), the magnetic structures of thousands of compounds have been investigated and reported. In 1976, an important effort was made to gather information available on all the magnetic structures known at that point,



© 2016 International Union of Crystallography

and a compilation of about 1000 magnetic structures was published (Oles *et al.*, 1976). This effort continued with an additional listing of about 100 structures in 1984 (Oles *et al.*, 1984). Since then, experimental facilities, instruments and analysis methods have improved enormously, and hundreds of magnetic structures are being reported each year. We estimate that, at the moment, there must be about 5000 published magnetic structures. In this scenario, the convenience of a digital database of magnetic structures seems clear, but despite some early work in this direction (Dul *et al.*, 1997), the lack of standards in the description and communication of magnetic structures has precluded the development of an appropriate computer database.

Two recent developments have, however, opened up new possibilities for the systematic application of magnetic symmetry and the achievement of a standardized framework for the description and digital storage of magnetic structures. Firstly, computer-readable listings of the magnetic space groups (or Shubnikov groups) have been made available (Litvin, 2013; Stokes & Campbell, 2011). Secondly, the superspace formalism (the standard approach for the quantitative description of non-magnetic incommensurate structures) has been extended in detail to incommensurate magnetic structures (Petříček *et al.*, 2010; Perez-Mato *et al.*, 2012). These fundamental steps have been the basis for the development of a series of computer tools for a comprehensive application of magnetic symmetry properties that allow an efficient crystallography-like methodology in the analysis and description of commensurate and incommensurate magnetic phases (Perez-Mato *et al.*, 2015). This methodology not only permits the exploration of the possible magnetic orderings associated with one or more propagation vectors in a form that complements and goes beyond the traditional representation method, but can also be employed to store and retrieve any magnetic structure in a robust and unambiguous form analogous to that employed for ordinary non-magnetic crystalline structures.

Another milestone has been the development by the Commission on Magnetic Structures of the IUCr (International Union of Crystallography, 2015) of the so-called magCIF format, *i.e.* an extension of the CIF (crystallographic information file) format (Brown & McMahon, 2002), which provides a robust and unambiguous file format for the archiving and exchange of magnetic structure information. Its preliminary version is already supported by the above-mentioned new symmetry-based computer tools.

Within this framework, we have collected at the Bilbao Crystallographic Server, under the name *MAGNDATA*, comprehensive information on more than 400 commensurate and incommensurate magnetic structures (Fig. 1). *MAGNDATA* is intended to be a benchmark and starting point for a complete database of magnetic structures, where magnetic symmetry is systematically employed and the magCIF format is the communication file format. Here, we present and discuss its main features for the case of commensurate structures. We concentrate on the information made available for each structure, and the way this information can be retrieved and analysed.

2. Description of commensurate magnetic structures

A magnetically long-range ordered structure can be considered fully determined if the available information unambiguously defines the average position of any atom and its average magnetic moment. In the case of a commensurate magnetic ordering, this can be achieved by providing three basic data items:

- (i) The lattice unit cell that defines the periodicity of the magnetic ordering, *i.e.* the so-called magnetic unit cell.
- (ii) The magnetic space group (MSG) or Shubnikov group, with the lattice described by (i), which defines the symmetry of the phase.
- (iii) The atomic positions (in relative units with respect to the unit cell) and magnetic moments (if the atom is magnetic) of a set of atoms in the unit cell that are not symmetry related and form an asymmetric unit. From these symmetry-independent atomic positions and magnetic moments, the position and magnetic moment of any other atom in the unit cell can be derived through the application of the symmetry operations of the MSG defined in (ii).

This is the basic information that is stored for any of the commensurate magnetic structures compiled in *MAGNDATA*, and it is an essential part of the corresponding magCIF file that can be downloaded. These magCIF files are supported by various programs, for example for visualization using *VESTA* (Momma & Izumi, 2011) and *Jmol* (Hanson, 2013), for editing using *ISOCIF* (Stokes & Campbell, 2015) or *STRCONVERT* (Perez-Mato *et al.*, 2015), for analysis using *ISODISTORT* (Campbell *et al.*, 2006), or for further refinement using experimental data and *FullProf* (Rodríguez-Carvajal, 1993) or *JANA* (Petříček *et al.*, 2014).

MAGNDATA: A Collection of magnetic structures with portable cif-type files

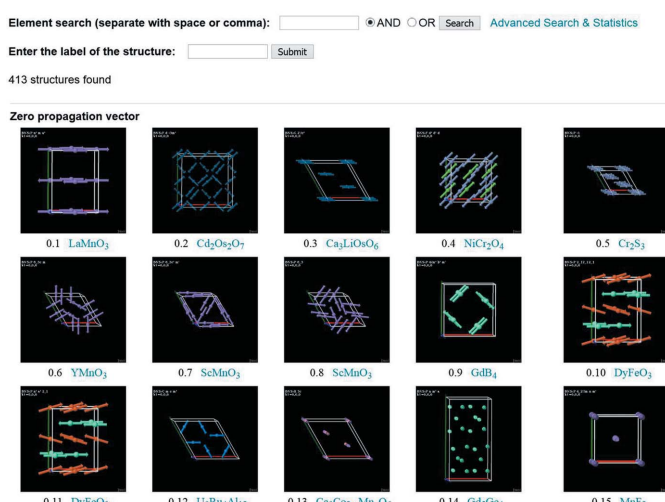


Figure 1

A screenshot showing a partial view of the online list with icons of the magnetic structures stored in *MAGNDATA*.

Table 1

Symmetry operations of the MSG describing the symmetry of the magnetic structure of $\text{Ba}_2\text{CoGe}_2\text{O}_7$ (#0.56; Hutana *et al.*, 2012).

These operations correspond to the MSG $Cm'm2'$ (No. 35.167) in a non-standard setting. The transformation to a standard setting is $(\mathbf{a} + \mathbf{b}, -\mathbf{a} + \mathbf{b}, \mathbf{c}; \frac{1}{2}, 0, 0)$.

No.	$x, y, z, \pm 1$	m_x, m_y, m_z	Seitz notation
1	$x, y, z, +1$	m_x, m_y, m_z	$[1 0]$
2	$y + \frac{1}{2}, x + \frac{1}{2}, z, +1$	$-m_y, -m_x, -m_z$	$[m'_{1\bar{1}0} \frac{1}{2}, \frac{1}{2}, 0]$
3	$-x, -y, z, -1$	$m_x, m_y, -m_z$	$[2'_{001} 0]$
4	$-y + \frac{1}{2}, -x + \frac{1}{2}, z, -1$	$-m_y, -m_x, m_z$	$[m'_{110} \frac{1}{2}, \frac{1}{2}, 0]$

As an example, Tables 1 and 2 present these three basic data items for the magnetic structure of $\text{Ba}_2\text{CoGe}_2\text{O}_7$ (Hutana *et al.*, 2012), which is depicted in Fig. 2(a), as retrieved from MAGNDATA, where it is entry 0.56. In the following, the entry number of each example in MAGNDATA will be indicated in parentheses with the symbol #, e.g. (#0.56). With respect to the data in these tables the following remarks are important.

2.1. Symmetry operations

The listed symmetry operations fully define the MSG of the structure. They are given in a similar form to the symmetry operations of space groups in conventional crystallography. Each symmetry operation is described by the corresponding transformation of a general position (x, y, z) (Hahn, 2002) (second column in Table 1) or in the Seitz notation (Glazer *et al.*, 2014) (last column in Table 1). These operations in the first format are the only obligatory data concerning symmetry in a magCIF file. The only difference with respect to the symmetry operations of ordinary space groups is that the presence or not in the symmetry operation of the action of time reversal is also indicated: in the first format this is achieved by means of an additional symbol, -1 or $+1$, while in the Seitz notation a prime symbol is added or not to the rotation or roto-inversion symbol. As additional (redundant) information, the transformation of a magnetic moment (given in relative components

Table 2

Positions and magnetic moments of symmetry-independent atoms in the magnetic structure of $\text{Ba}_2\text{CoGe}_2\text{O}_7$ (#0.56; Hutana *et al.*, 2012).

Unit cell $a = 8.46600$, $b = 8.46600$, $c = 5.44500$ Å, $\alpha = 90^\circ$, $\beta = 90^\circ$, $\gamma = 90^\circ$. MSG $Cm'm2'$ ($\mathbf{a} + \mathbf{b}, -\mathbf{a} + \mathbf{b}, \mathbf{c}; \frac{1}{2}, 0, 0$). Magnetic moment components are given in Bohr magnetons.

Magnetic atoms.

Label	Atom type	Atom			Multi-	Symmetry constraints			$ \mathbf{M} $	
		x	y	z		M_x	M_y	M_z		
Co	Co	0.0	0.0	0.0	2	$m_x, m_y, 0$	2.05	2.05	0.0	2.90

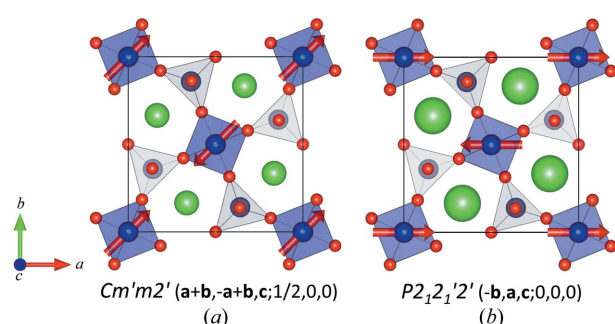
Non-magnetic atoms.

Label	Atom type	x	y	z	Multiplicity
Ba_1	Ba	0.83464	0.33466	0.50765	2
Ba_2	Ba	0.33464	0.16536	0.49235	2
Ge_1	Ge	0.64073	0.14073	0.95981	2
Ge_2	Ge	0.14073	0.35927	0.04019	2
O1_1	O	0.00000	0.50000	0.15942	1
O1_2	O	0.50000	0.00000	0.84058	1
O2_1	O	0.63791	0.13793	0.27045	2
O2_2	O	0.13791	0.36209	0.72955	2
O3_1	O	0.07906	0.18446	0.18857	4
O3_2	O	0.18446	0.92094	0.81143	4

with respect to the unit-cell basis) through the action of the symmetry operation is also listed (third column). The symmetry operations are described with respect to the magnetic unit cell that defines the lattice periodicity of the spin arrangement. In this sense, we use in all cases the Belov–Neronova–Smirnova (BNS) notation (Belov *et al.*, 1957). In the case of MSGs with antitranslations (*i.e.* operations combining a translation and time reversal), the alternative Opechowski–Guccione (OG) notation (Opechowski & Guccione, 1965) uses unit cells that are often closer to the reference lattice used in experiment, but in general they do not define the lattice periodicity of the MSG. The OG notation therefore requires a deviation from a straightforward extension of the group theoretical methods of ordinary crystallography, where symmetry operations and atomic variables are processed ‘modulo 1’ with respect to the employed unit cell. We have preferred to avoid this complication and therefore MAGNDATA has been developed in all aspects using the BNS approach.

2.2. Magnetic space groups

In most cases we have used a unit cell that keeps the origin and orientation of the crystallographic axes of the paramagnetic phase. This is the reason why, in most cases, as in this example, the MSG is in a non-standard setting. As the symmetry information provided by MAGNDATA is the list of symmetry operations in this non-standard basis, this causes no particular problem and no ambiguity exists. The transformation from the used basis to a basis corresponding to the standard setting of the MSG is given for each entry in the collection under the heading ‘Transformation to standard setting’.


Figure 2

(a) The magnetic structure of multiferroic $\text{Ba}_2\text{CoGe}_2\text{O}_7$ (Hutana *et al.*, 2012) retrieved from MAGNDATA (#0.56). A magnetically induced ferroelectric polarization along \mathbf{c} is symmetry allowed. (b) An alternative model with the same but rotated spin arrangement, which has different magnetic symmetry and no multiferroic character. The associated MSG is indicated below each panel. The basis transformation in parentheses beside the MSG label transforms the MSG to its standard setting.

In other words, the MSG defined by the listed operations in Table 1 is necessarily one of the 1651 Shubnikov groups, but its setting, *i.e.* the form of the operations, does not necessarily coincide with the one that is used in the listings of the MSGs that we can take as standard (Litvin, 2013; Stokes & Campbell, 2011; Bilbao Crystallographic Server, 2013). In the example above, if the change in unit cell and origin ($\mathbf{a} + \mathbf{b}$, $-\mathbf{a} + \mathbf{b}$, $\mathbf{c}; \frac{1}{2}, 0, 0$) is done, the symmetry operations transform into the BNS standard form of the MSG with the label $Cm'm2'$ and BNS number 35.167 (Bilbao Crystallographic Server, 2013). This means that the \mathbf{a}_o and \mathbf{b}_o basis vectors of the standard orthorhombic unit cell are given by the oblique vectors $\mathbf{a} + \mathbf{b}$ and $-\mathbf{a} + \mathbf{b}$, respectively, while the origin should be shifted by $\mathbf{a}/2$. We can summarize this information by saying, in short, that the symmetry of this structure is given by the MSG $Cm'm2'$ ($\mathbf{a} + \mathbf{b}$, $-\mathbf{a} + \mathbf{b}$, $\mathbf{c}; \frac{1}{2}, 0, 0$). Having computer-readable standard listings of all MSGs, this is the notation that can be used to define unambiguously any MSG under any setting. Notice, however, that the transformation to the standard setting is in general not unique, and different choices of unit cell and origin are possible for a standard setting of the MSG. In general, the transformation to standard setting given in each case is just one of the many possible ones.

The label provided for the relevant MSG is in fact not needed for describing the structure, as the listed set of symmetry operations of the MSG is sufficient to define the MSG that should be used to build up the full structure. The assignment of a standard label and a transformation to the MSG standard setting are, however, included in the magCIF file and in the database as additional complementary information. This summarizes the symmetry properties of the structure in a short unambiguous form and, for instance, the list of symmetry operations in Table 1 could be obtained by the application of the inverse of the transformation ($\mathbf{a} + \mathbf{b}$, $-\mathbf{a} + \mathbf{b}$, $\mathbf{c}; \frac{1}{2}, 0, 0$) to the BNS standard form of the operations of the MSG $Cm'm2'$ (No. 35.167), which are retrievable from the databases available on the internet (Bilbao Crystallographic Server, 2013; Stokes & Campbell, 2011). Thus Table 2, with its heading that defines the unit cell, and the MSG label together with the transformation to its standard setting, can be considered a complete, unambiguous and robust form to report the magnetic structure, without the need for Table 1.

2.3. The metrics of the unit cell

As the paramagnetic phase is tetragonal and no orthorhombic strain has been detected, the unit cell of the example above has tetragonal metrics despite the MSG being orthorhombic. This is a common situation, as magnetoelastic couplings are usually very weak and the symmetry break, which in principle is relevant for all degrees of freedom, is often not observed in the lattice. However, it is important to know that, according to the symmetry of the phase, an orthorhombic strain of the unit cell is possible. From the orientation of the standard unit cell of the MSG, one can see that this symmetry-allowed strain is in fact a shear strain,

Table 3

Full set of symmetry-related atoms in the unit cell, and their magnetic moments, generated from the symmetry-independent Co atom listed in Table 2 (*MAGNDATA* #0.56), as retrieved from *MAGNDATA*.

Atom	<i>x</i>	<i>y</i>	<i>z</i>	Symmetry constraints on <i>M</i>	<i>M_x</i>	<i>M_y</i>	<i>M_z</i>
1	0.00000	0.00000	0.00000	$m_x, m_y, 0$	2.05	2.05	0.0
2	0.50000	0.50000	0.00000	$-m_y, -m_x, 0$	-2.05	-2.05	0.0

namely a deviation of the γ angle from 90° , while the a and b parameters must keep equal values.

2.4. Positions and magnetic moments of the symmetry-independent magnetic atoms

The magnetic moments of the magnetic atoms are given as components (in Bohr magnetons) along the \mathbf{a} , \mathbf{b} and \mathbf{c} unit-cell basis vectors. Other alternative parameterizations of the magnetic moments are included in the magCIF dictionary, but they have not been implemented in this database. As shown in Table 2, we list not only the positions and magnetic moments of the symmetry-independent magnetic atoms, but also the symmetry constraints acting on the magnetic moments. It can then be seen that, although according to the model the magnetic moments are aligned along the $(1, 1, 0)$ direction, a deviation from this direction is symmetry-allowed.

2.5. Positions and magnetic moments of all atoms in the unit cell

Optionally, *MAGNDATA* provides the positions and magnetic moments of all the atoms in the unit cell. They are derived from those in the asymmetric unit using the symmetry operations of the MSG: if \mathbf{r} and \mathbf{m} are the position and magnetic moment, respectively, of an atom in the asymmetric unit, a symmetry operation $\{\mathbf{R}|\mathbf{t}\}$ implies the presence of another atom of the same species at $\mathbf{r}' = \mathbf{R}\mathbf{r} + \mathbf{t}$, with magnetic moment given by $\det(\mathbf{R})\mathbf{R} \cdot \mathbf{m}$, while if the symmetry operation is $\{\mathbf{R}'|\mathbf{t}\}$, *i.e.* it includes time reversal, the magnetic moment has an additional change of sign and is given by $-\det(\mathbf{R}')\mathbf{R} \cdot \mathbf{m}$. The listing that can be retrieved for the magnetic atoms of our example is shown in Table 3. One can see in this table that the additional symmetry-allowed moment component in the orthogonal direction $(1, \bar{1}, 0)$ breaks the collinearity of the spin configuration and is ferromagnetic. Thus, one can predict from the symmetry assignment that this structure is bound to exhibit weak ferromagnetism on the ab plane, more specifically along $(1, \bar{1}, 0)$. The possible existence of weak ferromagnetism can also be derived directly from the magnetic point group symmetry associated with the MSG (see below).

2.6. Atomic positions of non-magnetic atoms

In principle, the MSG of a commensurate magnetically ordered phase describes the symmetry constraints of all degrees of freedom, not only of the magnetic ones. Thus, the atomic positions of all the non-magnetic atoms are also derived from those listed within the asymmetric unit by the

action of the MSG operations, knowing that the presence or not of time reversal in the operation is irrelevant for the non-magnetic degrees of freedom. The positions and occupancies of all atomic sites are therefore subject to an effective ordinary space group that can be derived from the relevant MSG by eliminating the presence or not of time reversal in its operations. The effective space group in the above example is therefore *Cmm2* ($\mathbf{a} + \mathbf{b}$, $-\mathbf{a} + \mathbf{b}$, $\mathbf{c}; \frac{1}{2}, 0, 0$), with the same transformation to its standard description as for the MSG. As the parent paramagnetic phase of this compound has space group *P42₁m*, some atomic sites are split with respect to the paramagnetic structure, and this is reflected in the listing of Table 2 with the split atoms having composite numbers in their labels, such as O1_1, O1_2 etc. Also, the unsplit Co atomic site acquires some additional freedom, as the position is now free along the polar \mathbf{c} direction. The atomic positions listed in Table 2 reflect all the positional degrees of freedom released by the magnetic ordering that could in principle be relevant if the magnetostructural coupling becomes important. It is in the framework of this effective symmetry break *P42₁m* \rightarrow *Cmm2* for the non-magnetic degrees of freedom that the multiferroic properties of this material can be explained (Perez-Mato & Ribeiro, 2011).

In most cases, the magnetostructural coupling is very weak and the symmetry break for the positional structure associated with the magnetic ordering, even if formally present, remains undetected within the accuracy of the experimental data. Thus, it is usual that the atomic positions of a magnetic structure are modelled within a good approximation using the constraints associated with the symmetry of the paramagnetic phase, independently of the magnetic ordering producing or not a symmetry break for the atomic positions. Most magnetic structures are therefore refined considering the positional structure and the spin configurations as two separate phases, with the positional structure being modelled under the space group of the paramagnetic phase. Often, the positional structure is even assumed to be identical to that determined in the paramagnetic phase. Although this type of approximation is often justified, a unique common rigorous approach to all structures, including those where a significant magnetostructural coupling is observed, seemed more appropriate for a database. We have therefore preferred to describe in all cases all the degrees of freedom, both for atomic positions and magnetic moments, under the symmetry constraints of the MSG that is relevant for the reported magnetic arrangement. This is the case for the example above where, despite having an observable electric polarization, the accompanying structural distortion was too weak to be detected and the positional structure was reported under the space group *P42₁m*. Therefore, the symmetry-split atomic sites in Table 2 corresponding to an effective *Cmm2* space group are only virtual and have been derived from the reported *P42₁m* positional structure. This may seem inefficient for some purposes, but it has the advantage of making explicit the structural degrees of freedom that become free in the magnetic phase and which must be taken into account in any eventual investigation of magnetostructural effects.

2.7. Transformation from the original published data

A good number of the magnetic structures published in the past or being published at present are determined using the representation method (Bertaut, 1968; Izyumov *et al.*, 1991) without making use of or identifying the MSG of the resulting magnetic structure. This has meant that, in many cases, we had to reinterpret the spin arrangement of the original article and transform it to the crystallographic symmetry-based description explained above. In this process, the identification of the symmetry group of the reported structure was essential.

In order to identify the relevant MSG, instead of applying a brute force search, a deductive process starting from the knowledge of the parent symmetry and the propagation vector(s) was followed. In most cases, this basic knowledge was sufficient to reduce the possible MSGs to a quite limited set of subgroups of the grey magnetic group associated with the parent phase. These MSGs have a hierarchy according to their group–subgroup relations, and are readily obtained using computer tools such as *MAXMAGN* or *k-SUBGROUPS-MAG*, also available on the Bilbao Crystallographic Server (Perez-Mato *et al.*, 2015). Using these programs, combined if necessary with *MAGMODELIZE*, also available there, the different spin-ordering models corresponding to the alternative possible symmetries could be obtained in a straightforward manner and compared with the reported structure. In this way, the relevant symmetry was in general easily identified, and in most cases it was one of the (few) maximal subgroups in the hierarchical tree of possible MSGs (see §5 for an example). Once the appropriate magnetic symmetry had been identified, the above-mentioned tools were also employed to produce an appropriate magCIF file of the magnetic structure.

2.8. Visualization and analysis

The output page for each structure includes a pair of figures obtained with *VESTA* (Momma & Izumi, 2011). One of the figures depicts all the atoms, while the second reduces the graphical representation to the magnetic atoms. The *VESTA* files corresponding to these figures can also be downloaded, but in any case the latest versions of *VESTA* support the magCIF format and commensurate magnetic symmetry. Therefore, the magCIF file provided by *MAGNDATA* can be

MAGNDATA Structure Viewer: 3D Visualization of magnetic structures with Jmol

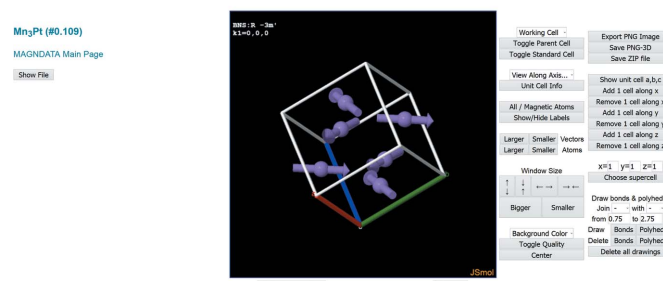


Figure 3

A screenshot of the online visualization of Mn₃Pt (Krén *et al.*, 1967) (#0.109).

used directly as input for *VESTA*, which can be used to visualize/analyse the structures.

A direct link to an online three-dimensional viewer that uses *Jmol* (Hanson, 2013) is also available (see Fig. 3). This online tool makes directly accessible the simplest and most important commands of *Jmol* through specific buttons, while the innumerable commands available to manipulate and analyse the graphical representation can be applied through a command window or pop-up console. The latest version of *Jmol* fully supports MSGs and accepts magCIF files as input files. Therefore, *Jmol* can also be used locally if the magCIF file of the structure is downloaded, provided that the user has previously installed this free program.

3. Additional information

Apart from the minimal information necessary to build up the magnetic structure in three-dimensional space, *MAGNDATA* provides additional important data. This information is also included in the corresponding magCIF file that can be retrieved (local tags beyond the official magCIF dictionary are used for some of the items). We list and discuss here the most important items

3.1. Magnetic point group

The magnetic point group (MPG) associated with a commensurate magnetic structure can be derived in a straightforward manner from the knowledge of its MSG, simply by taking the rotation or roto-inversion operations combined (or not) with time reversal present in the group. This is a very important piece of information, as the magnetic point group governs the macroscopic crystal tensor properties. For instance, the point group of $\text{Ba}_2\text{CoGe}_2\text{O}_7$ (#0.56) discussed above is $m'm'2'$ (No. 7.3.2) (Litvin, 2013) (in a non-standard setting). *MAGNDATA* explicitly lists the operations of the magnetic point group in the used setting (see Table 4).

A direct link to *MTENSOR* (another program on the Bilbao Crystallographic Server) then allows the user to explore, for this specific point group and the setting used, the symmetry-adapted form of any macroscopic tensorial magnetic, structural or magnetostructural property (see next section). For the simplest properties in this example the results are rather obvious: the point group is polar along the **c** direction, while it allows ferromagnetism along the **b** direction of the standard unit cell, *i.e.* the $(\bar{1}, 1, 0)$ direction in the basis used. The parent symmetry being non-polar, the magnetic point group symmetry is thus sufficient for the characterization of the system as having a non-polar/polar symmetry break and therefore as a type II multiferroic, where one can expect some induced electric polarization and some weak ferromagnetism, in accordance with the discussion in §2.

One must be aware that, in general, the point group symmetry of a magnetic structure not only is determined by the spin arrangement but also depends on the positions of the non-magnetic atoms: the simple spin arrangement depicted in Fig. 2(a), if considered in a purely mono-atomic Co structure,

Table 4

Symmetry operations of the magnetic point group of $\text{Ba}_2\text{CoGe}_2\text{O}_7$ (Hutana *et al.*, 2012) as given in *MAGNDATA* (#0.56).

These operations form the magnetic point group $m'm'2'$ (No. 7.3.2) in a non-standard setting. The transformation to a standard setting is $\mathbf{a} + \mathbf{b}$, $-\mathbf{a} + \mathbf{b}$, \mathbf{c} .

No.	$x, y, z, \pm 1$	m_x, m_y, m_z	Seitz notation
1	$x, y, z, +1$	m_x, m_y, m_z	1
2	$y, x, z, +1$	$-m_y, -m_x, -m_z$	$m_{1\bar{1}0}$
3	$-x, -y, z, -1$	$m_x, m_y, -m_z$	$2'_{001}$
4	$-y, -x, z, -1$	$-m_y, -m_x, m_z$	m'_{110}

would have implied a rather different MSG and point group, which would forbid both ferroelectricity and weak ferromagnetism. Only the presence of the non-magnetic atoms reduces the parent symmetry, and as a consequence also the symmetry of the magnetic structure, to the MSGs discussed above.

It is also important to remark that both the MSG and the corresponding magnetic point group, and therefore also the multiferroic properties of this particular example, depend on the orientation of the collinear spin arrangement (see Fig. 2). The MSG, and as a consequence the magnetic point group, change if this orientation is changed. For instance, if the spins align along the **a** direction, the MSG changes to $P2_12_12'$ ($-\mathbf{b}$, **a**, **c**; 0, 0, 0), with point group $2'2'2'$ (**a**, $-\mathbf{c}$, **b**), which is non-polar, but it also has a ferromagnetic (FM) component allowed along the **b** direction, perpendicular to the direction of the antiferromagnetic (AFM) arrangement (Perez-Mato & Ribeiro, 2011). An electric polarization is not possible for this configuration and therefore magnetically induced ferroelectricity, which can be present for the oblique orientation of the spins, is forbidden for this alternative orientation. One can then predict that an external magnetic field rotating on the *ab* plane, through its coupling with the weak FM component, should induce the rotation of the AFM spin arrangement and a switch between the two limiting polar and non-polar symmetries, producing a sinusoidal oscillation of the induced electric polarization along **c**. This is indeed what is observed experimentally (Murakawa *et al.*, 2010).

Although the magnetic anisotropy may favour some specific direction, and hence some specific MSGs, it is sometimes difficult, as in this example, to determine the absolute orientation of the spins and, even if that is experimentally feasible, this orientation may be easily manipulated with external fields. In practice, this can mean some uncertainty over the actual MSG of the magnetic phase and the corresponding point group. In these ambiguous cases, we have generally assumed a spin orientation that maximizes the resulting magnetic symmetry. Known macroscopic properties, as shown in this example, can help to avoid ambiguities over the relevant MSG.

3.2. Parent space group and relation of the basis used to that of the parent phase

By definition, a magnetic structure is distorted with respect to a so-called parent structure without magnetic order. This is independent of the magnetic phase being accessible directly

from a paramagnetic phase or being bordered in the phase diagram by other magnetic phases. Although a magnetic structure is in principle fully defined using the data discussed in the previous section, the knowledge of the symmetry of its parent paramagnetic structure is fundamental to characterize the possible domains and the switching properties of the system. Therefore, this parent space group is included as additional information. If the parent structure has been considered in a non-standard setting, the transformation of its basis to the standard setting is also given.

In the above example of $\text{Ba}_2\text{CoGe}_2\text{O}_7$ (#0.56), the parent space group is $P\bar{4}2_1m$, with the same unit cell and origin as those employed to describe the magnetic structure. This means that the magnetic phase results from a symmetry break that can be represented as

$$P\bar{4}2_1m \rightarrow Cm'm2'(\mathbf{a}_p + \mathbf{b}_p, -\mathbf{a}_p + \mathbf{b}_p, \mathbf{c}_p; \frac{1}{2}, 0, 0), \quad (1)$$

where the transformation to the standard setting is now described with respect to the basis of the parent phase. The index of the MSG $Cm'm2'$, as a subgroup of the parent grey tetragonal magnetic space group $P\bar{4}2_1m1'$ of the paramagnetic phase, is 4, and therefore four domain types are possible. Removing the trivial ones related by time reversal and having all spins reversed, one has to consider two distinct non-trivial domains related, for instance, by the lost operation $\{\bar{4}_{001} | 0, 0, 0\}$. This means that the two domains will have their spins rotated by 90° and opposite electric polarization along \mathbf{c} . This switching property is directly related to the symmetry of the parent phase. A magnetic structure with the same symmetry $Cm'm2'$, and for instance a parent space group $Cmmm1'$, would have different switching properties, having the spins in the two non-trivial domains related by space inversion.

The database includes information about the relation of the bases used for the reference parent phase and the magnetic unit cell. This is given under the heading ‘Transformation from parent structure’. In the example above this transformation is the identity, *i.e.* $(\mathbf{a}, \mathbf{b}, \mathbf{c}; 0, 0, 0)$. As a more complex example, we show in Fig. 4 the case of $\text{Ba}_3\text{Nb}_2\text{NiO}_9$ (Hwang *et al.*, 2012) (#1.13). Here, the parent space group is $P\bar{3}m1$ and the propagation vector of the magnetic ordering is $(\frac{1}{3}, \frac{1}{3}, \frac{1}{2})$. The magnetic unit cell that we use keeps the orientation and origin

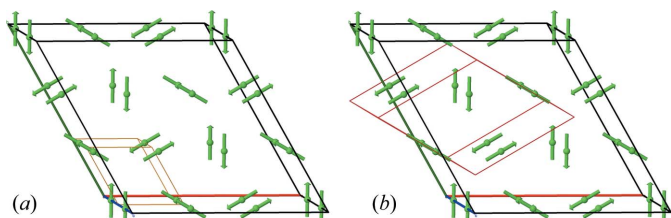


Figure 4

The spin arrangement in the magnetic structure of $\text{Ba}_3\text{Nb}_2\text{NiO}_9$ (#1.13) reported by Hwang *et al.* (2012), as given by the online *Jmol* visualization tool of MAGNDATA, showing (a) the magnetic unit cell used and the parent unit cell, and (b) the magnetic unit cell used and that corresponding to the standard setting of the MSG.

of the parent unit cell. Therefore, the indicated ‘Transformation from parent structure’ is $(3\mathbf{a}, 3\mathbf{b}, 2\mathbf{c}; 0, 0, 0)$. This is not a standard setting for the MSG P_c31c of the structure, and under the heading ‘Transformation to a standard setting’ the transformation $(\frac{2}{3}\mathbf{a} + \frac{1}{3}\mathbf{b}, -\frac{1}{3}\mathbf{a} + \frac{1}{3}\mathbf{b}, \mathbf{c}; \frac{1}{3}, \frac{2}{3}, 0)$ is indicated. One should be aware that the first transformation refers to the parent basis, while the second one refers to the working magnetic unit cell that is being used for the MSG. The three bases/unit cells can be visualized online, as shown in Fig. 4. Combining the two basis transformations (from parent unit cell to the used magnetic unit cell, and from the used magnetic unit cell to a magnetic unit cell in a standard setting), the symmetry break between the parent and the magnetic phase is fully defined. Thus, in this example, the symmetry break is

$$P\bar{3}m11' \rightarrow P_c31c(2\mathbf{a}_p + \mathbf{b}_p, -\mathbf{a}_p + \mathbf{b}_p, 2\mathbf{c}_p; \frac{1}{3}, \frac{2}{3}, 0), \quad (2)$$

In most cases, the parent space group is clearly defined, as it corresponds to the symmetry of the experimental paramagnetic phase, and this structure is usually known and used as a reference for the subsequent determination of the magnetic structure. However, if the paramagnetic structure also includes some structural distortion with respect to a higher symmetry, the concept of parent symmetry becomes ambiguous and the formal choice of a parent space group is not unique. In these cases, we have usually considered as the parent structure the one that was used as a reference for the magnetic diffraction in the article reporting the structure. However, in some exceptional cases a better choice was detected and a different parent symmetry has been considered. This may happen, for instance, in magnetic phases where the presence of a concomitant structural distortion has led to the use of the distorted structure as a reference for the refinement of the magnetic diffraction data.

3.3. Propagation vector(s)

The propagation vectors that are active as primary wavevectors of the magnetic ordering are part of the characterization of a magnetic phase. These wavevectors can be derived in a straightforward manner from knowledge of the MSG and the parent space group of the magnetic structure, and the relation of their respective unit-cell bases. In practice, however, the propagation vectors are directly accessible in diffraction experiments, and knowledge of them is usually the first step in the process of determining the magnetic structure. Thus, although the form in which the magnetic structures are described in MAGNDATA does not require the explicit definition of these propagation vectors, this information is included as an important complementary feature which is directly related to the experiment. If the magnetic arrangement includes spin waves with wavevectors corresponding to harmonics of a primary propagation vector, they are also listed.

The components of the propagation vectors are given in the reciprocal conventional basis of the parent space group. In our first example of Fig. 1, the propagation vector is $\mathbf{k} = (0, 0, 0)$, which means that magnetic ordering keeps the lattice of the

parent structure, and neutron magnetic diffraction peaks will superpose with the nuclear ones. In Fig. 4, the propagation vector is $(\frac{1}{3}, \frac{1}{3}, \frac{1}{2})$.

The propagation vectors are used in this collection as the most basic feature for classifying the magnetic structures, and this is reflected in the entry labels. The structures are divided into six fundamental classes:

Class 0. Magnetic structures with a null propagation vector [$\mathbf{k} = (0, 0, 0)$] which keep the lattice of the parent structure, and their MSG is necessarily of type I or III (Bradley & Cracknell, 1972), which means that the MSG does not include antitranslations of type $\{1'|\mathbf{t}\}$ (*i.e.* combinations of translations with time reversal).

Class 1. Commensurate magnetic structures with a single primary nonzero propagation vector \mathbf{k} , such that $n\mathbf{k}$ is a reciprocal lattice vector of the parent space group, with n even. The MSGs of these structures are necessarily of type IV (Bradley & Cracknell, 1972), *i.e.* they contain anti-translations of type $\{1'|\mathbf{t}\}$. Higher harmonics with wavevectors $m\mathbf{k}$ (m odd) may be present in the spin arrangement (if these vectors are not equivalent to \mathbf{k}). The point group of these materials includes time reversal, *i.e.* it is a grey point group, and therefore linear magnetostructural effects are not possible.

Class 1.0. Commensurate magnetic structures with a single primary nonzero propagation vector \mathbf{k} , such that $n\mathbf{k}$ is a reciprocal lattice vector of the parent space group, with n odd. The MSGs of these structures are necessarily of type I or III (Bradley & Cracknell, 1972), as in Class 0, but some lattice translations of the parent structure are lost and the lattice of the magnetic structure is described by a supercell of the parent unit cell. As in the previous class, higher harmonics with wavevectors $m\mathbf{k}$ (m odd) can be present in the spin arrangement, and in this case these possible higher harmonics necessarily include a wavevector equivalent to $(0, 0, 0)$. This means that some magnetic neutron diffraction peaks can superpose with the nuclear ones if such a harmonic is present in the spin arrangement.

Class 2. Commensurate magnetic structures with two independent primary propagation vectors.

Class 3. Commensurate magnetic structures with three independent primary propagation vectors. Among the structures in classes 2 and 3 with more than one primary propagation vector, those having propagation vectors that are symmetry-related by the MSG operations form an important special set. However, the number of multi- \mathbf{k} magnetic structures that are being reported is minimal, and therefore we have not introduced further divisions within classes 2 and 3.

Class 1.1. Incommensurate magnetic structures with a single primary incommensurate propagation wavevector. The symmetry of magnetic structures with incommensurate propagation wavevectors cannot be described using an MSG or Shubnikov group. Their systematic description requires a different methodology. Its symmetry can be described by a magnetic superspace group (MSSG), similar to what happens in the case of incommensurate non-magnetic crystals and quasicrystals (Perez-Mato *et al.*, 2012). The specific form in which incommensurate magnetic structures are stored in

MAGNDATA using magnetic superspace symmetry is described in detail in a separate publication (Gallego *et al.*, 2016).

3.4. Representation analysis

Commensurate magnetic structures are described in this database under the framework and constraints associated with their MSG, without using the so-called representation method (Bertaut, 1968; Izyumov *et al.*, 1991). However, once a magnetic structure is described under its relevant MSG symmetry and a corresponding magCIF file is prepared, the symmetry mode decomposition of the magnetic structure with respect to the parent structure, in terms of basis spin modes corresponding to the different possible irreducible representations (irreps) of the parent space group, can be done in a straightforward manner with the program ISODISTORT (Campbell *et al.*, 2006). Following this procedure, we have obtained for most structures of this collection their irrep mode decomposition, and we have included a brief summary of the magnetic irreps that are active in each phase and their restrictions. Only in the trivial cases for which the assignment of the MSG has a one to one correspondence with the assignment of an irrep has this step often been skipped.

Table 5 lists a set of examples of the information provided on the irrep mode decomposition. The irrep labels are those provided by ISODISTORT. This labelling convention is robust and unambiguous, and can be applied through computer-readable irrep listings (Stokes *et al.*, 2013). It has been adopted by the Bilbao Crystallographic Server and by JANA (Petříček *et al.*, 2014). This irrep labelling is also consistent with the most extended notation for \mathbf{k} vectors corresponding to symmetry points, lines and planes of the Brillouin zone (Aroyo *et al.*, 2014). Note that the irreps associated with spin modes, which are odd for time reversal, are distinguished from the analogous non-magnetic ones, which are even for time reversal, by means of the letter ‘m’ as a prefix. For each active irrep, the dimensions of the small and the full representations are given. The factor between these two numbers is the number of \mathbf{k} vectors in the star of the irrep (Bradley & Cracknell, 1972; Stokes *et al.*, 2013).

If the irrep is multidimensional, the direction of the magnetic order parameter in irrep space is classified as either ‘general’ or ‘special’. A ‘general’ order parameter direction indicates that the MSG allows any arbitrary combination of the irrep spin basis modes and the MSG is the minimum magnetic symmetry compatible with this irrep distortion, *i.e.* the so-called kernel of the irrep, in contrast with the higher symmetries for some specific irrep subspaces, the so-called irrep epikernels (Ascher, 1977). If the order parameter direction is termed ‘special’, we mean that the symmetry constraints of the MSG imply the restriction to some specific linear combinations of the irrep spin basis modes, and therefore the spin degrees of freedom of the magnetic phase are fewer than those provided by the full set of irrep spin basis functions.

Table 5Examples of the information available on the symmetry mode decomposition of the magnetic structures in *MAGNDATA*.

Compound	Reference [†]	Parent space group	k vector(s)	Magnetic space group	Irrep(s)	$d_s\ddagger$	$d_i\$$	Order parameter direction	Action
MnTe ₂ (#0.20)	(a)	$P\bar{a}\bar{3}$	(0, 0, 0)	$P\bar{a}\bar{3}$ (No. 205.33)	mGM1	1	1		Primary
LiFeGe ₂ O ₆ (#1.39)	(b)	$P2_1/c$	($\frac{1}{2}$, 0, 0)	$P_{a2_1/c}$ (No. 14.80)	mY1+	1	1		Primary
ErAuGe (#1.33)	(c)	$P6_3mc$	($\frac{1}{2}$, 0, 0)	P_{Cna2_1} (No. 33.154)	mm2	1	3		Primary
Mn ₃ Pt (#0.109)	(d)	$Pm\bar{3}m$	(0, 0, 0)	$R\bar{3}m'$ (No. 166.101)	mGM4+	3	3	Special	Primary
Na ₂ MnF ₅ (#1.55)	(e)	$P2_1/c$	(0, $\frac{1}{2}$, 0)	P_{bc} (No. 7.29)	mZ1	2	2	Special	Primary
HoMnO ₃ (#1.20)	(f)	$Pnma$	($\frac{1}{2}$, 0, 0)	P_{bmn2_1} (No. 31.129)	mX1	2	2	Special	Primary
TbMn ₂ O ₅ (#1.108)	(g)	$Pbam$	($\frac{1}{2}$, 0, $\frac{1}{4}$)	C_{am} (No. 8.36)	mG1	2	4	General	Primary
Ca ₃ LiOsO ₆ (#0.3)	(h)	$R\bar{3}c$	(0, 0, 0)	$C2'/c'$ (No. 15.89)	mGM3+	2	2	Special	Primary
					mGM2+	1	1		Secondary
NiO (#1.6)	(i)	$Fm\bar{3}m$	($\frac{1}{2}$, $\frac{1}{2}$, $\frac{1}{2}$)	$C_{c2/c}$ (No. 15.90)	mL3	2	8	Special	Primary
					mL2+	1	4		Secondary
TmAgGe (#3.1)	(j)	$P\bar{6}2m$	($\frac{1}{2}$, 0, 0) ($\frac{1}{2}$, $\frac{1}{2}$, 0) (0, $\frac{1}{2}$, 0)	$P\bar{6}'2m'$ (No. 189.224)	mm2	1	3	Special-2	Primary
FePO ₄ (#0.17)	(k)	$Pnma$	(0, 0, 0)	$P_{2_12_12_1}$ (No. 19.25)	mGM1+	1	1		Primary
					mGM1-	1	1		Primary
Bi ₂ MnRuO ₇ (#0.153)	(l)	$Fd\bar{3}m$	(0, 0, 0)	$Fd'd'd$ (No. 70.530)	mGM4+	3	3	Special	Primary
					mGM5+	3	3	Special	Primary
LuFe ₄ Ge ₂ (#0.140)	(m)	$P4_2/mnm$	(0, 0, 0)	$Pn'n'm$ (No. 58.399)	mGM2-	1	1		Primary
					GM2+	1	1		Primary
					mGM1-	1	1		Secondary

[†] References: (a) Burlet *et al.* (1997), (b) Redhammer *et al.* (2009), (c) Baran *et al.* (2001), (d) Krén *et al.* (1967), (e) Núñez *et al.* (1994), (f) Muñoz, Casáis *et al.* (2001), (g) Blake *et al.* (2005), (h) Calder *et al.* (2012), (i) Ressouche *et al.* (2006), (j) Baran *et al.* (2009), (k) Rousse *et al.* (2003), (l) Martínez-Coronado *et al.* (2014), (m) Schobinger-Papamantellos *et al.* (2012). [‡] Dimension of small irrep. ^{\$} Dimension of full irrep.

In the case of irreps with more than one arm in their star of **k** vectors and with **k** equivalent to $-\mathbf{k}$, spin arrangements restricted to a single **k** imply a special direction for the order parameter of a rather trivial character. This restriction is introduced automatically in the traditional representation method, when the exploration of spin arrangements is limited to those coming from the spin basis functions associated with a single **k** of the irrep star. Non-trivial symmetry constraints in **1k** magnetic structures that are not included in the traditional representation method appear when the star of **k** vectors includes the vector $-\mathbf{k}$ as non-equivalent and/or when the small irrep is multidimensional. In both cases, the irrep restricted to the symmetry operations that either keep **k** invariant or change it into $-\mathbf{k}$ (the so-called extended small space group) is multidimensional. The effective order parameter for the single-**k** spin arrangements is therefore multidimensional in these cases and, for special directions within the order parameter space, a higher MSG (irrep epikernel) may be realized. These are the cases that are indicated in the database as having a ‘special’ direction for the irrep, and they are of interest because the correspondence between the MSG and the irrep assignment is not one to one, with different MSGs being possible for the same active irrep.

In the case of multi-**k** structures with several propagation vectors belonging to the same irrep star, even if the small irrep is one dimensional and **k** is equivalent to $-\mathbf{k}$, special directions of the order parameter with different MSGs can occur, depending on the way the spin basis functions corresponding to different propagation vectors of the irrep star are combined. These structures are distinguished in the database

by denoting them as ‘special-2’ for the direction of the order parameter.

The information on the irrep mode decomposition is completed with the qualification of the active irreps which are listed as ‘primary’ or ‘secondary’. A symmetry-allowed irrep distortion is identified as primary if the spin modes can be considered as the driving agent for the symmetry break of the magnetic phase, while it is secondary if they are symmetry allowed but their presence in the magnetic ordering can be considered a secondary induced effect, which could be negligible.

In most cases, only one irrep is compatible with the MSG of the structure, and therefore its primary character is obvious. This is the case for the first seven examples in Table 5, where one can see that, when the small irrep is multidimensional, in most cases the magnetic phase corresponds to a special irrep direction, and therefore the description using the MSG implies additional constraints. Other structures have an MSG that is compatible with more than one magnetic irrep [see Ca₃LiOsO₆ (#0.3; Calder *et al.*, 2012) and subsequent entries in Table 5], but one of the possible irreps is the primary one, yielding the symmetry break in the observed MSG. The distinction between primary and secondary irreps has relevance only in this type of structure. Secondary irrep distortions, although symmetry-allowed, are usually absent. They can appear as weak secondary induced effects, and they are often negligible. The absence of these secondary irrep distortions implies that the effective number of spin degrees of freedom of the structure decreases, with respect to those allowed by the MSG, by constraining the model to the spin

degrees of freedom of the primary irrep. However, it is important to remark that, in the traditional refinement method, the possible presence of allowed secondary irreducible distortions may have been discarded *a priori* without an experimental check. A combined application of magnetic symmetry and representation analysis is especially recommended in these structures. Representation analysis allows the decomposition of the spin degrees of freedom within the relevant MSG into primary and secondary ones, and the performance of a controlled and systematic check of the significance of possible secondary modes in the spin arrangement. However, the identification of the relevant MSG for the phase is a necessary previous step in order to ‘symmetry adapt’ the spin basis modes of the primary irrep.

The explicit separation of the magnetic degrees of freedom into primary and secondary ones (if these latter exist) within the constraints of an MSG can be done using *ISODISTORT*. In *MAGNDATA*, we have only included some information about the number of degrees of freedom associated with each irrep, and a flag indicating whether the secondary irrep is really present with nonzero amplitude in the distortion. This information does not pretend to be comprehensive. In any case, users can always download the corresponding magCIF and, with the CIF of the appropriate parent phase, obtain in a few minutes with *ISODISTORT* (and previous transformation with *ISOCIF* if the magCIF file is in a non-standard setting) the symmetry mode decomposition of any of the commensurate structures in *MAGNDATA*. A direct link to another program on the Bilbao Crystallographic Server also provides a survey of all compatible irreps (see next section).

Magnetostructural coupling is usually too weak to allow observation of secondary non-magnetic structural displacive distortion modes induced by the magnetic ordering. If they exist in the reported structure, they have generally not been included in the summary of the irrep mode decomposition of the structure, which is limited to the magnetic irreps. Non-magnetic irreps have only exceptionally been included in the irrep summary, as for instance in the case of LuFe₄Ge₂ (#0.140; Schobinger-Papamantellos *et al.*, 2012). This compound is reported to exhibit a structural phase transition simultaneously with the magnetic ordering. From its symmetry properties one can deduce that the observed structural distortion is not a magnetic induced effect, as this distortion produces an additional symmetry break that must be taken into account for the MSG of the magnetic phase. Therefore, the non-magnetic irrep associated with this structural distortion should be considered as a primary irrep, and it is listed accordingly in the irrep summary.

3.5. Transition temperature and experiment temperature

If available, the transition temperature below which the reported structure becomes stable is given. This usually coincides with the Néel temperature of a paramagnetic–antiferromagnetic phase transition, but in systems with multiple magnetic phases the temperature given can be the upper temperature bordering a neighbouring magnetic phase.

If available, the temperature at which the magnetic diffraction data were measured (experiment temperature) is also listed.

3.6. References

Magnetic structures are often reported without providing a detailed account of the atomic positional structure that has been considered, or if provided, it may correspond to the paramagnetic phase or to a measurement at a different temperature from the one at which the magnetic ordering was measured. In order to have as complete a description of the magnetic structure as possible, we have in most cases used (if available) the atomic positions from the same reference, as retrieved from the Inorganic Crystal Structure Database (ICSD, 2007), and the ICSD entry number is indicated. If not available, an ICSD entry for the same compound (usually at room temperature) has been employed. In other cases the positional structure has been manually retrieved from the reference. In general, one should be aware that atomic positions are often only approximate, as they may have been determined independently of the magnetic ordering and under different experimental conditions.

3.7. Comments

The comments that appear for a particular structure are normally reduced to information on the experimental technique used for the data, details of the experimental conditions or the phase diagram of the material, the existence of similar structures *etc*. If the MSG corresponds to a so-called \mathbf{k} -maximal symmetry (Perez-Mato, 2015) (see next section), this is also stated in the comments. The presence of a magnetic structure in this collection should not be taken as a kind of validation, as we have not performed any cross-check of the proposed structures, and the only requirement was that the model is self-consistent and unambiguous. In fact, the database contains more than one model for some magnetic phases, and they do not necessarily agree. If, according to our analysis, a structure presents some contradictions, compared with either the information given in the same publication or that in other references, these problems are mentioned in the comments. If the way that the structure has been reported strongly indicates that it was fitted without fully exploring all possible spin arrangements, or introducing some strong aprioristic constraints, this may also be mentioned here.

4. Links to other programs

By means of direct links, the relevant data for any entry can be introduced for further analysis into other programs of the Bilbao Crystallographic Server. The most important linked programs are the following:

STRCONVERT. This tool allows automatic online editing, some transformations and different output formats.

MAGNEXT (Gallego *et al.*, 2012). This program provides the systematic absences to be expected on the non-polarized neutron magnetic diffraction diagram due to the MSG of the crystal. The program can also list the symmetry-forced form of

the magnetic structure factor for special symmetry directions or planes in reciprocal space. This information can be used to derive additional systematic absences if the orientation of the spins has constraints that are not dictated by the MSG. Possible extra systematic absences due to the restrictions of the magnetic sites to some specific Wyckoff positions are not included. It is important to remark that the systematic absences are expressed in terms of (h, k, l) indices with respect to the reciprocal unit cell of the basis used for the description of the magnetic structure in the present database. This unit cell does not necessarily coincide with that considered in the original publication.

MTENSOR. This program provides the symmetry-adapted form of any crystal tensor property (equilibrium, optical or transport properties). All kinds of crystal tensors (up to eighth rank) can be consulted. The tensor constraints are derived considering the magnetic point group of the structure in the setting (in general non-standard) defined by the unit cell used in the present database. For example, Fig. 5 reproduces the output of *MTENSOR* for the linear magnetoelectric tensor relating electric polarization and magnetic field for the case of Ba₂CoGe₂O₇ (#0.56), the example discussed in §2. From the form of the magnetoelectric tensor, one can derive that the application of a magnetic field along \mathbf{c} is bound to induce some electric polarization along the (1, 1, 0) direction, which is the direction of the weak ferromagnetism. Alternatively, the application of the magnetic field along this particular basal direction induces some electric polarization along \mathbf{c} , which should be added to the ferroelectric spontaneous polarization along this direction. Although in general this magnetoelectric response may be difficult to disentangle from additional magnetoelectric effects due to field-induced reorientation of the spins and domain switching, one must be aware of its existence when interpreting magnetoelectric experiments. Through this link with *MTENSOR*, our database provides the necessary information for any kind of crystal tensor property that may be of interest. This program can also be used to explore tensor switching properties when switching the system to domain-related configurations.

MVISUALIZE. Apart from being a *Jmol*-based visualization tool, with similar features to the online viewer mentioned in §2, this separate program, which can work with any magnetic structure introduced with a magCIF file, can be used to produce domain-equivalent structures or to change the

αT_{ij}	j		
i	1	2	3
1	0	0	αT_{13}
2	0	0	$-\alpha T_{13}$
3	αT_{31}	$-\alpha T_{31}$	0

Figure 5

The symmetry-adapted form of the magnetoelectric tensor (inverse effect) relating electric polarization and magnetic field, in the form $P_i = \alpha^T_{ij}H_j$, for Ba₂CoGe₂O₇ (*MAGNDATA* #0.56) as given by *MTENSOR* through its link with *MAGNDATA*. Note that the setting of the orthorhombic point group symmetry is not standard.

description of the structure to any setting/unit-cell basis that may be wished, including the standard setting.

From the knowledge of the parent space group and the MSG of the structure, the program provides a complete set of parent symmetry operations that, applied to the original structure, produce all possible distinct domain-related equivalent structures. These alternative domain-related equivalent descriptions of the magnetic structure can then be visualized and saved as magCIF files.

Let us consider the case of Cs₂CoCl₄ (#1.51; Kenzelmann *et al.*, 2002). The symmetry break of the magnetic ordering in this compound is

$$Pnma1' \rightarrow P_a2_1'(\mathbf{c}_p, \mathbf{a}_p, \mathbf{b}_p + \mathbf{c}_p; 0, \frac{3}{8}, -\frac{1}{8}), \quad (3)$$

with the propagation vector $\mathbf{k} = (0, \frac{1}{2}, \frac{1}{2})$. The primitive magnetic cell is duplicated with respect to that of the parent lattice, while the point group symmetry reduces from the 16 operations of *mmm1'* to the four operations in *21'*. Hence the index of the magnetic group, as a subgroup of the parent grey group, is 8 and we should expect eight types of domain. The domain-related structures are obtained by transforming the structure stored in the database by the lost symmetry operations of the paramagnetic phase. Only a coset representative for each of the eight cosets of the coset decomposition of the MSG *P_a2₁* with respect to the parent group *Pnma1'* is necessary to obtain the eight distinct domain-related configurations of the magnetic structure with respect to the parent paramagnetic phase. After elimination of the trivial domains obtained by switching all spins to opposite values by the action of the lost time reversal, there are then four non-trivial domains. This means that four distinct but equivalent descriptions of the magnetic structure exist if the parent paramagnetic phase is taken as a common reference. *MVISUALIZE* makes a choice for this set of distinct non-trivial coset representatives (see Fig. 6) and provides, if desired, the magnetic structure models corresponding to each of them (see Fig. 7).

Enumeration of the different domain-related descriptions is very important when comparing structures proposed by

Domain-related equivalent descriptions

MAGNDATA entry: Cs₂CoCl₄ (#1.51)

Magnetic space group: *P_a2₁* (#4.10) (c,a,1/2b+1/2c; 0,3/8,-1/8)
Parent space group: *Prima* (#62) (a,b,c; 0,0,0)
Transformation from parent structure: (a,2b,2c; 0,0,0)

[Magnetic Structure]

Domain-related equivalent structures: coset representatives and conjugated subgroups

The transformation matrices of the table are from the parent space group to the standard setting of the listed magnetic space groups
The coset representatives used to derive the domain-related equivalent structures are expressed in the setting of the parent group

N	Coset representatives (x,y,z) form	Seitz notation	Transformation matrix	Magnetic Structure
1	x,y,z,+1	{1 0}	$\begin{pmatrix} 0 & 1 & 0 & 0 \\ 0 & 0 & 1 & 3/4 \\ 2 & 0 & 1 & 7/4 \end{pmatrix}$	Show
2	-x+1/2,-y,z+1/2,+1	{2001 1/2 0 1/2}	$\begin{pmatrix} 0 & 1 & 0 & 0 \\ 0 & 0 & 1 & 3/4 \\ 2 & 0 & 1 & 7/4 \end{pmatrix}$	Show
3	-x,-y,-z,+1	{-1 0}	$\begin{pmatrix} 0 & 1 & 0 & 0 \\ 0 & 0 & 1 & 3/4 \\ 2 & 0 & 1 & 7/4 \end{pmatrix}$	Show
4	x+1/2,y,-z+1/2,+1	{m001 1/2 0 1/2}	$\begin{pmatrix} 0 & 1 & 0 & 0 \\ 0 & 0 & 1 & 3/4 \\ 2 & 0 & 1 & 7/4 \end{pmatrix}$	Show

Figure 6

A screenshot of the output for Cs₂CoCl₄ (#1.51) listing the chosen set of symmetry operations (coset representatives) in the magnetic phase, whose action on the magnetic structure produces all the distinct non-trivial domain-related spin arrangements, which are physically equivalent.

different studies or when refining the structure. It allows the researcher to enumerate all possible models that are experimentally indistinguishable because of their full equivalence. Particularly in the case of powder diffraction, it is not uncommon to confuse or mix these alternative descriptions of the same model with physically different ones that may fit the experimental data equally well. A systematic determination of all domain-related descriptions not only precludes this confusion, but can also help to detect pseudosymmetry in the model. In Fig. 6 for instance, one can see that the inversion symmetry is only broken by the slight canting of the spins. But the spin z component of the Co atoms is 0.4 (2) Bohr magnetons, compared with 1.6 (4) for the y component (Kenzelmann *et al.*, 2002). The spin canting that breaks the centrosymmetry of the structure is therefore close to its standard deviation. Cs_2CoCl_4 (#1.51) is one of the few magnetic structures in *MAGNDATA* where the spin arrangement associated with a single multidimensional irrep corresponds to a general direction within the irrep, and the symmetry is reduced to the irrep kernel (see Table 6 in §6).

Get_mirreps. This program provides a list of compatible irreps for a given magnetic symmetry break from a parent grey group. It includes all magnetic and non-magnetic irreps of the parent grey group that are allowed to be active in a distorted structure with the symmetry given by the input subgroup. The corresponding wavevectors and special directions within the irrep spaces are also indicated. Through the direct link to this program, one obtains for each commensurate structure

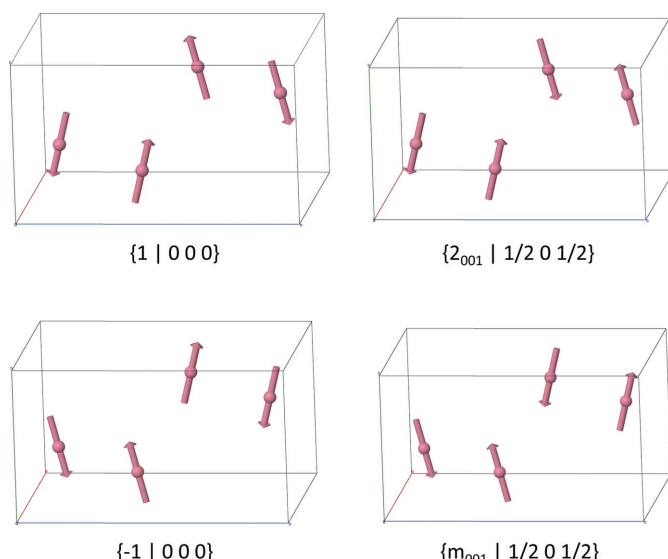


Figure 7

Graphical representation of the four non-trivial domain-related equivalent descriptions of the magnetic structure of Cs_2CoCl_4 (#1.51), as obtained using the corresponding link in *MAGNDATA*. Only the magnetic atoms within a parent unit cell are shown. The spins are repeated in consecutive parent cells with the same or opposite orientation, according to the set of centring translations and anti-translations of the corresponding MSG or, equivalently, according to the phase factor for the propagation vector $\mathbf{k} = (0, \frac{1}{2}, \frac{1}{2})$. The lost symmetry operation (coset representative listed in Fig. 6) that has been employed to generate the transformed structure is indicated below each case. Four additional domains, trivially related to those in the figure through the switch of the direction of all spins, complete the set.

information about all possible primary and secondary irreps that can be relevant. It should be stressed that the program lists *all* compatible irreps from the viewpoint of symmetry, without considering the specificity of the structure. This means that some of these irreps may be irrelevant, because they are not present in the irrep decomposition of the degrees of freedom of the structure.

5. Trend to maximal symmetry: the example of pyrochlore-type structures

A general principle of maximal symmetry is generally at work, and the symmetry of the majority of the structures that are being reported is given by a ‘maximal subgroup’ among the set of possible ones. These most favourable MSGs can be termed ‘maximal’ in the sense that there is no supergroup (subgroup of the parent grey symmetry) that fulfils the same conditions. If only the compatibility condition with the observed propagation vector(s) is taken into account, we denote these most favourable MSGs as ‘ \mathbf{k} -maximal subgroups’, ‘ \mathbf{k} -maximal MSGs’, ‘ \mathbf{k} -maximal symmetries’ etc. (Perez-Mato *et al.*, 2015). However, the compatibility condition can be more restrictive if the magnetic atoms occupy special Wyckoff positions, and some of the MSGs compatible with the observed propagation vector(s) can be discarded, either because they force a null magnetic moment at all magnetic sites or because they do not represent any additional degree of freedom with respect to those already allowed by a supergroup.

As an example, Fig. 8 shows the possible MSGs for a magnetic structure with parent space group $Fd\bar{3}m$ (parent MSG $Fd\bar{3}m1'$), zero propagation vector, and magnetic atoms at the positions $16c$ $(0, 0, 0)$ and/or $16d$ $(\frac{1}{2}, \frac{1}{2}, \frac{1}{2})$. The figure shows the group–subgroup hierarchy among all the possible symmetries which could be realized. This is the relevant scenario for all magnetic orderings in pyrochlore-type structures that do not break the parent lattice periodicity. In the figure, one can see that there are six possible maximal symmetries in the sense explained above, and three of them are realized in some of the collected structures. Fig. 9 depicts some examples. Although we could not find any experimental structure with any of the other three maximal symmetries, one should be aware that these magnetic structures are often determined with ‘trial and error’ methods, and in some cases it is doubtful that all possible alternative arrangements have been explored and cross-checked. In other cases, powder diffractometry is unable to distinguish between alternative spin modes or their combination, and an arbitrary choice has been made among indistinguishable (but different) configurations (Wills *et al.*, 2006).

Only three of the ten pyrochlore-type zero-field magnetic phases with $16c$ or $16d$ as the magnetic site and with $\mathbf{k} = 0$, which are present in *MAGNDATA*, do not possess a maximal symmetry in the sense explained above. Two of them have the symmetry $I4_1/am'd$. As shown in Fig. 8, this group is a subgroup of $Fd\bar{3}m'$ and is therefore not maximal among the possible subgroups. It is, however, maximal among the possible symmetries for magnetic ordering if, according to

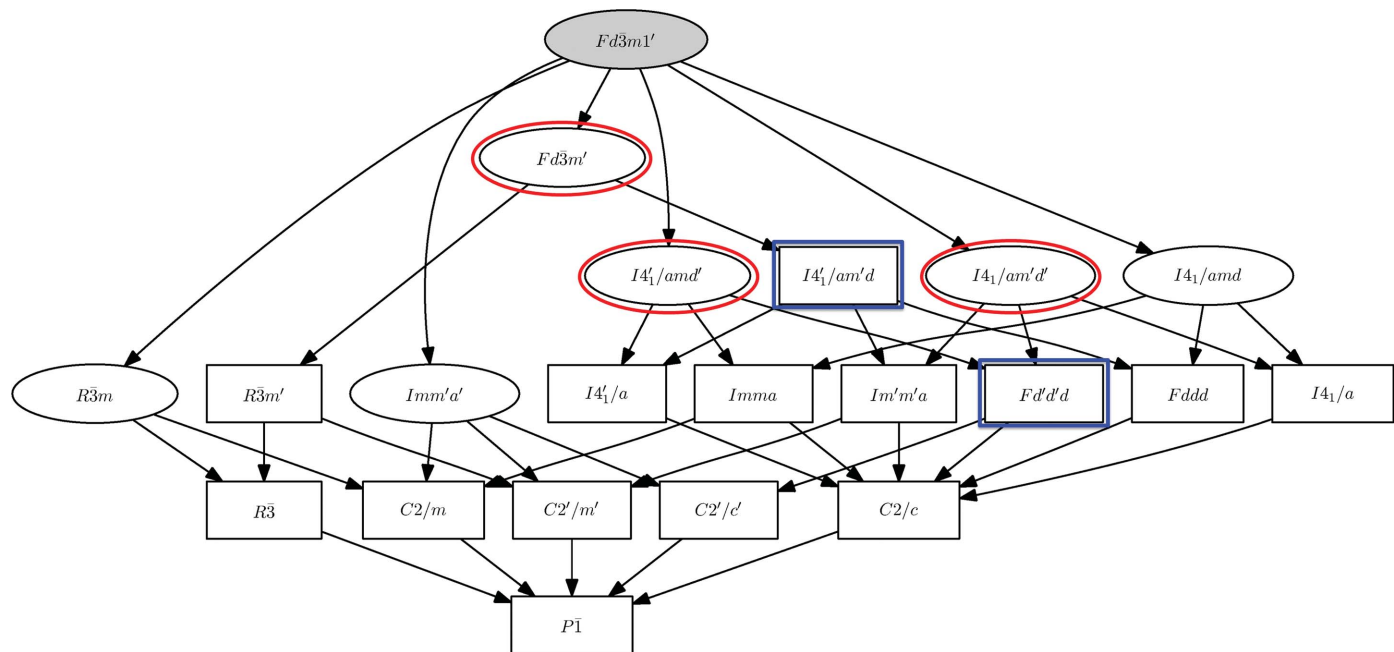


Figure 8

Possible symmetries for a magnetic structure having a parent structure with space group $Fd\bar{3}m$ and a null propagation vector, with the magnetic atoms at sites $16c$ ($0, 0, 0$) and/or $16d$ ($\frac{1}{2}, \frac{1}{2}, \frac{1}{2}$). The symmetries are shown as subgroups of the parent grey MSG using standard BNS labels (Stokes & Campbell, 2011), indicating their group–subgroup relationship. Maximal subgroups are surrounded by black ovals. Only one MSG is shown for each conjugacy class of physically equivalent subgroups. The symmetries realized by the experimental pyrochlore structures gathered in MAGNDATA are highlighted with blue ellipses in the case of maximal symmetries or with blue squares otherwise. (Obtained with *k*-SUBGROUPSMAG; Perez-Mato *et al.*, 2015.)

Landau theory (see §3 above), it is assumed to be triggered by a single irrep. As shown in Fig. 10, this subgroup is indeed one of the two possible maximal symmetries resulting from a spin arrangement according to the two-dimensional irrep GM3+. In general, all maximal MSGs for a given propagation vector and specific magnetic sites are maximal irrep epikernels, but the reverse is not true. Some irrep epikernels of maximal symmetry may be subgroups of one or more MSGs, which are epikernels (or kernels) for another irrep. This is the case in Fig. 10 for the MSG $I4'_1/am'd'$, which is a subgroup of $Fd\bar{3}m'$, the kernel of irrep mGM2+ (see Fig. 8). This means that this MSG allows the presence of a secondary mGM2+ spin mode

of symmetry $Fd\bar{3}m'$, apart from the primary irrep mode corresponding to mGM3+.

The structure of $\text{Bi}_2\text{RuMnO}_7$ (#0.153; Martínez-Coronado *et al.*, 2014) is the only one of the pyrochlore-type structures that could not be classified as having maximal symmetry, in the broad sense summarized in Fig. 8, or in the restrictive sense of a maximal epikernel of a single irrep, as described by Fig. 10. As can be seen in the irrep decomposition summary of this simple collinear structure, this model represents the superposition of spin modes corresponding to two different irreps, namely mGM4+ and mGM5+ (see Table 5), and it is therefore not simple from this viewpoint. It is not clear if the collinearity

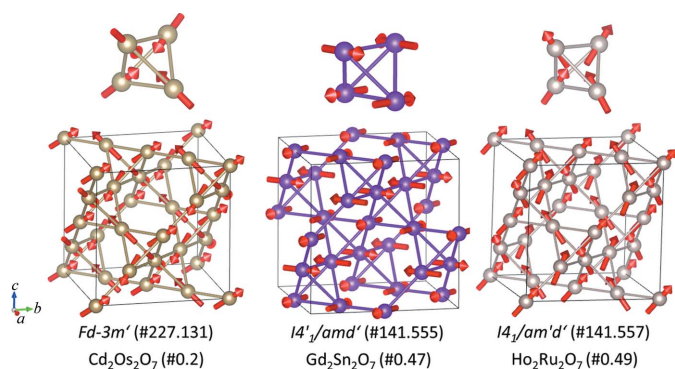


Figure 9

Examples of magnetic structures in MAGNDATA having one of the maximal symmetries indicated in Fig. 8, corresponding to $\text{Cd}_2\text{Os}_2\text{O}_7$ (Yamaura *et al.*, 2012), $\text{Gd}_2\text{Sn}_2\text{O}_7$ (Wills *et al.*, 2006) and $\text{Ho}_2\text{Ru}_2\text{O}_7$ (Wiebe *et al.*, 2004).

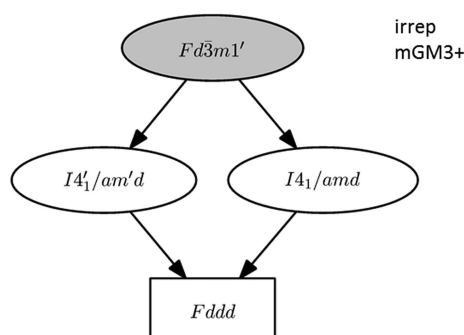


Figure 10

Possible MSGs (epikernels and kernel) for spin arrangements according to the two-dimensional irrep mGM3+ of $Fd\bar{3}m$ (#227), with $\mathbf{k} = 0$, showing their group–subgroup relationship. Maximal subgroups are surrounded by black ovals. One single group for each conjugacy class of equivalent subgroups is shown. (Obtained with *k*-SUBGROUPSMAG; Perez-Mato *et al.*, 2015.)

was an *a priori* assumption or whether more complex models were explored during the refinement. In any case, the authors reporting the structure seem to be unaware of the fact that the proposed collinear model, despite its apparent simplicity, implies the presence of two active primary irreps.

From this example, it becomes clear that an efficient methodology for the structure determination of such a type of complex phase would require the systematic contrast of the experimental data with each of the models corresponding to *all* possible alternative maximal symmetries, monitoring within these symmetries the degrees of freedom corresponding to different irreps if more than one is allowed, and eventually descending to lower MSGs, if necessary.

6. A survey of the collection

MAGNDATA includes a set of sampling and search tools that can be used to explore various properties among the more than 370 collected commensurate structures. Here, we summarize some of the features that can be explored with these tools.

6.1. Experimental technique

While neutron powder diffraction is the main technique for the determination of most of the structures, about one-fifth of them are based on data from neutron single-crystal experiments.

6.2. Structures with a single active primary one-dimensional irrep

About 95% of the structures are single-**k** structures, and 50% of them have a one-dimensional order parameter transforming according to an irrep which is one-dimensional when restricted to the subspace of spin arrangements with the observed propagation vector. In the language of representation analysis, this means that the small irrep is one-dimensional and the propagation vectors **k** and $-\mathbf{k}$ are equivalent. These are the most simple magnetic structures. The MSG is necessarily **k** maximal in the sense explained in previous sections, and space inversion symmetry is necessarily conserved if existing in the parent phase. Apart from the domains corresponding to possible symmetry-related distinct propagation vectors, only two types of domain exist, which are trivially related by time reversal (switch of all the spins).

6.3. Structures with a single primary multidimensional irrep active

About 100 single-**k** structures have a primary irrep which is multidimensional when restricted to the subspace of spin arrangements for the given propagation vector. The relevant MSG in about 80% of these structures corresponds to an irrep epikernel of maximal symmetry (see §§4 and 5). This means that the spin arrangement includes symmetry-dictated constraints restricting the possible combination of the irrep basis functions. In these structures, the effective point group for the non-magnetic degrees of freedom is lower than the set

of parent point group operations keeping the propagation vector invariant, and non-trivial orientational domains with the same propagation vector exist.

6.4. Structures with maximal symmetry

About 76% of the single-**k** commensurate structures have a **k**-maximal symmetry, and if one adds those with their symmetry given by a maximal epikernel of a multidimensional irrep that is not **k** maximal, the number of structures with maximal symmetry within the constraint of a **k** vector or irrep is about 85%. There are therefore about 15% of structures with symmetries that are not maximal in either of these two senses. These cases require either the action of two or more primary irreps or some arbitrariness in the direction taken by the magnetic order parameter, which in these exceptional cases would not be fully dictated by symmetry.

6.5. Structures with exceptionally low symmetries

We could only detect eight structures where the direction of the magnetic order parameter within the multidimensional irrep is ‘general’ in the sense explained in §4, such that it does not take one of the possible symmetry-dictated directions of higher symmetry. These are listed in Table 6. Most of them are rather complex structures with many spin degrees of freedom, even if they are restricted to a single active irrep [see, for instance, DyFe₄Ge₂ (#1.98; Schobinger-Papamantellos *et al.*, 2006) and Tm₅Ni₂In₄ (#1.170; Szytula *et al.*, 2014) in Fig. 11]. Often, the articles accompanying the reports of these structures suggest that the MSG of the model has not been monitored, and models with possible higher symmetries associated with the epikernels of the irrep have not been explored and contrasted with the proposed structure. In some cases, the macroscopic properties of the phases also suggest the possibility of a higher MSG and therefore a special direction for the order parameter. This happens, for instance, with the multiferroics BiMn₂O₅ (#1.75; Vecchini *et al.*, 2008), and TbMn₂O₅ (#1.108) and HoMn₂O₅ (#1.109; Blake *et al.*, 2005), where the direction of the induced electric polarization is along one of the orthorhombic directions, which would be consistent with one of the irrep epikernels. In the case of BiMn₂O₅, such an

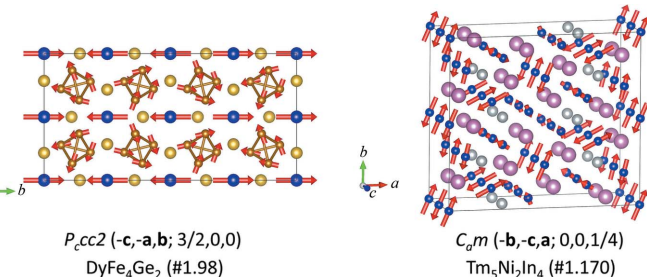


Figure 11

The magnetic structures of DyFe₄Ge₂ (Schobinger-Papamantellos *et al.*, 2006) and Tm₅Ni₂In₄ (Szytula *et al.*, 2014) as retrieved from *MAGNDATA* (#1.98 and #1.170). These models belong to the few (listed in Table 6) where the magnetic symmetry realized is not maximal for the active irrep.

Table 6

Single- \mathbf{k} magnetic structures where the multidimensional order parameter takes a general direction and the symmetry is not maximal for the relevant irrep.

The dimension of the irrep restricted to the subspace of the \mathbf{k} vector is given in the last column in parentheses, together with the label of the irrep.

Compound	Reference†	\mathbf{k} vector	Parent space group	Magnetic space group	Magnetic point group	Irrep (dimension)
Cs ₂ CoCl ₄ (#1.51)	(a)	(0, $\frac{1}{2}$, $\frac{1}{2}$)	Pnma	P _a 2 ₁ (No. 4.10)	21'	mT1 (2)
BiMn ₂ O ₅ (#1.75)	(b)	($\frac{1}{2}$, 0, $\frac{1}{2}$)	Pbam	C _d m (No. 8.36)	m1'	mU1 (2)
DyFe ₄ Ge ₂ (#1.98)	(c)	($\frac{1}{4}$, $\frac{1}{4}$, 0)	P4 ₂ /mnm	P _c cc2 (No. 27.82)	mm21'	mSM4 (2)
TbMn ₂ O ₅ (#1.108)	(d)	($\frac{1}{2}$, 0, $\frac{1}{4}$)	Pbam	C _d m (No. 8.36)	m1'	mG1 (4)
HoMn ₂ O ₅ (#1.109)	(d)	($\frac{1}{2}$, 0, $\frac{1}{4}$)	Pbam	C _d m (No. 8.36)	m1'	mG1 (4)
NiSb ₂ O ₆ (#1.113)	(e)	($\frac{1}{2}$, 0, $\frac{1}{2}$)	P4 ₂ /mnm	P _S $\bar{1}$ (No. 2.7)	$\bar{1}\bar{1}'$	mR1+ (2)
NiS ₂ (#1.167)	(f)	($\frac{1}{2}$, $\frac{1}{2}$, $\frac{1}{2}$)	P \bar{a} 3	P _S $\bar{1}$ (No. 2.7)	$\bar{1}\bar{1}'$	mR1+R3+ (4)
Tm ₃ Ni ₂ In ₄ (#1.171)	(g)	(0, $\frac{1}{2}$, $\frac{1}{2}$)	Pbam	C _d m (No. 8.36)	m1'	mT1 (2)

† References: (a) Kenzelmann *et al.* (2002), (b) Vecchini *et al.* (2008), (c) Schobinger-Papamantellos *et al.* (2006), (d) Blake *et al.* (2005), (e) Ehrenberg *et al.* (1998), (f) Yano *et al.* (2016), (g) Szytula *et al.* (2014).

alternative structure of higher symmetry has in fact been reported in another study (#1.74; Muñoz *et al.*, 2002).

Among this set of structures of exceptionally low symmetry, there are also quite simple ones such as Cs₂CoCl₄ (#1.51;

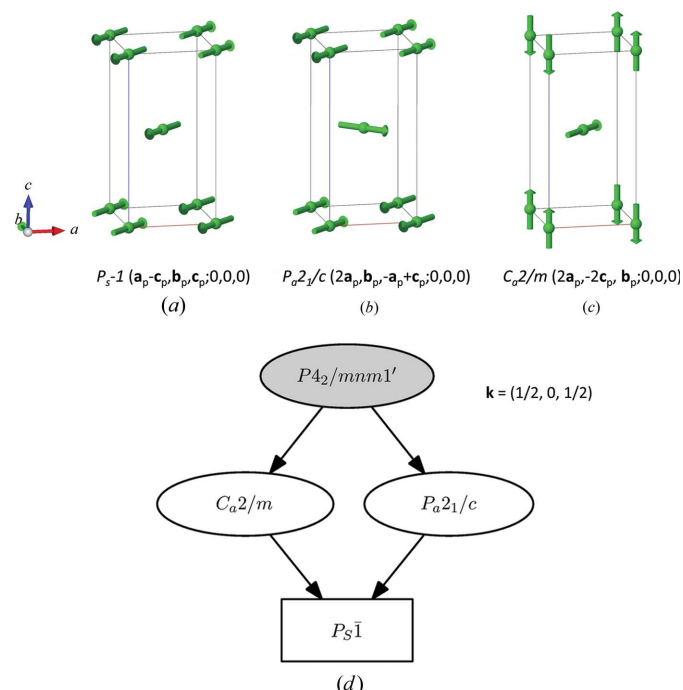


Figure 12

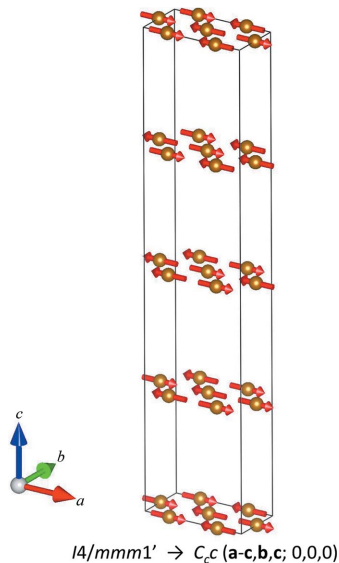
(a) A scheme of the collinear magnetic structure reported for NiSb₂O₆ (Ehrenberg *et al.*, 1998) (#1.113) with the lowest possible symmetry, despite its collinearity. Only the spins in a parent unit cell are shown; the signs of the spins in consecutive unit cells are determined by the propagation vector ($\frac{1}{2}$, 0, $\frac{1}{2}$). Its MSG, and a transformation from the parent tetragonal basis to its standard setting, are indicated below the sketch. The magnetic sites at the origin and at the unit-cell centre are symmetry independent and have their three spin components fully free. (b) and (c) Alternative models with higher symmetry according to the group–subgroup hierarchy of possible subgroups shown in part (d). In the P_a2_1/c symmetry the two Ni sites are symmetry related, only one having its three spin components free, and the arrangement is necessarily non-collinear, except if the easy axis is either along \mathbf{b} or on the ac plane. In the case of the MSG C_o2/m the two sites are independent, with one having the spin restricted along \mathbf{c} and the other on the ab plane, also forcing either a non-collinear arrangement or a null spin in one of the magnetic atoms.

Kenzelmann *et al.*, 2002), already discussed in §4 (see Fig. 7), where the general direction and the deviation from an MSG of higher symmetry are due to a small spin canting, close to its standard deviation. The spin arrangement of NiSb₂O₆ (#1.113; Ehrenberg *et al.*, 1998), depicted in Fig. 12(a), is also very simple, but its simplicity is deceptive from the point of view of magnetic symmetry. Non-collinear arrangements could conserve higher symmetries, which correspond to the epikernels of the only possible active irrep. Sketches of these alternative models are also shown in Fig. 12. Certainly, the prevalence of the exchange interaction in conjunction with crystal anisotropy may favour the reported collinear arrangement, despite its larger symmetry reduction. Nevertheless, sometimes it seems that the non-collinear models corresponding to possible higher symmetries have not been fully checked.

It should be remarked that there are also a few structures where the order parameter direction is termed ‘general’ in the database, but the irrep is a two-dimensional so-called ‘physically irreducible’ representation. Two-dimensional physically irreducible representations do not possess special directions of higher symmetry and have no epikernel, the maximal symmetry being the irrep kernel, realized for any direction of the order parameter. Therefore, in these cases, a general direction for the order parameter is the only one possible, and they have not been included in Table 6.

6.6. Structures with several primary irreps

Most of the structures are the consequence of an order parameter transforming according to a single primary irrep, in agreement with the usual assumption based on the Landau theory of phase transitions. However, about 10% require the action of two or more primary irreps. Table 5 lists the example of FePO₄ (#0.17; Rousse *et al.*, 2003), where the spin arrangement includes spin modes corresponding to two one-dimensional irreps, the resulting MSG being the intersection of the kernels of the two irreps, and therefore both irreps being primary. The reason for the presence of two primary irreps is often quite obvious, like the existence of two consecutive phase transitions, or the independent ordering of two

**Figure 13**

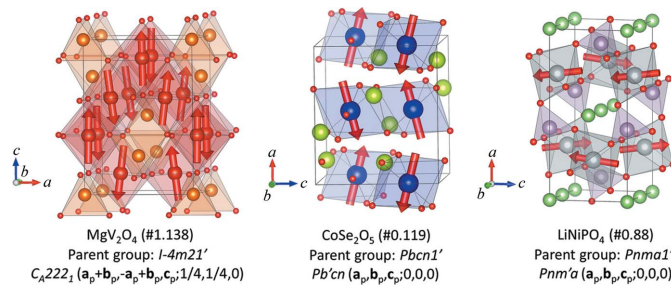
The collinear magnetic structure of $\text{La}_2\text{O}_2\text{Fe}_2\text{OSe}_2$ (Free & Evans, 2010) (#1.58) with an indication of the symmetry break with respect to the paramagnetic phase. Two active primary irreps for the wavevector $(\frac{1}{2}, 0, \frac{1}{2})$ are required in order to have non-null spins at all magnetic sites and the symmetry reduces to a polar monoclinic MSG, with potential multiferroic properties.

different magnetic atoms, but in other cases it is not clear and would require deeper investigation.

The case of $\text{La}_2\text{O}_2\text{Fe}_2\text{OSe}_2$ (#1.58; Reehuis *et al.*, 2011) shown in Fig. 13 is especially remarkable. This simple collinear arrangement with propagation vector $(\frac{1}{2}, 0, \frac{1}{2})$ involves two primary irreps and breaks the space inversion of the parent phase with space group $I4/mmm$. The reason is that any of the irreps, if considered alone, would force a null spin in half of the magnetic sites, which are located at Wyckoff position $4c$ of the parent phase. Therefore, the collinear ordering of all atoms is sufficient here to yield a symmetry break into polar symmetry and the system, being a semiconductor, could be expected to exhibit type II multiferroic properties with spin-driven ferroelectricity (Perez-Mato *et al.*, 2016). A similar situation, where the reported collinear arrangement requires two primary irreps, happens in $\text{Bi}_2\text{RuMnO}_7$ (#0.153; Martínez-Coronado *et al.*, 2014), already discussed in §5.

6.7. Collinearity and canting

About 50% of the collected structures are collinear, as expected from the usually dominant exchange-type interactions. In contrast with the unusual example of Fig. 13, these collinear arrangements are often compatible with one of the maximal MSGs. Their collinearity can even be part of the constraints of the MSG and in such cases it is symmetry protected [see, for instance, LiFePO_4 (#0.95; Rousse *et al.*, 2003) or CrN (#1.28; Corliss *et al.*, 1960)]. In most cases, however, the MSG allows spin components that can break the collinearity. In such cases, assuming collinearity reduces the effective number of spin degrees of freedom with respect to those really allowed by the relevant MSG. The identification

**Figure 14**

Examples of magnetic structures retrieved from MAGNCDATA [MgV_2O_4 (#1.138; Wheeler *et al.*, 2010), CoSe_2O_5 (#0.119; Melot *et al.*, 2010) and LiNiPO_4 (#0.88; Jensen *et al.*, 2009)] with significant spin canting compatible with their MSG. Below each figure, the parent grey group and the MSG of the structure are indicated, including the transformation from the parent basis to the standard setting of the MSG.

of the MSG identifies these possible spin cantings, which are often too weak to be detected, especially in powder experiments. Nevertheless, the collection in MAGNCDATA includes a good number of structures where they are significant and have been fully characterized (see Fig. 14 for some examples). These structures mostly come from single-crystal studies and it is noticeable that, among the structures that have been determined from single-crystal data, the models with collinearity that is not forced by symmetry amount to only about 10%. This percentage is much larger among the structures determined from powder data.

An exceptional case is CoSe_2O_5 , where the results seem to be in contradiction with the general trend: while a powder diffraction study (Melot *et al.*, 2010) reported the structure represented in Fig. 14, with a considerable symmetry-allowed spin canting, a more recent single-crystal study (#0.161; Rodriguez *et al.*, 2016) has refuted the existence of any observable deviation from collinearity.

6.8. Weak ferromagnetics and ferrimagnetics

Any antiferromagnetic phase with a magnetic point group compatible with homogeneous magnetization is susceptible to exhibiting weak ferromagnetism. In other words, weak ferromagnetism can appear in any AFM phase where the cancelling of the global magnetization is not symmetry dictated. In most cases, the symmetry-allowed FM component is too weak to be observed in diffraction experiments, but it is in general detectable in macroscopic measurements. There are about 100 structures with MSGs allowing ferromagnetism, among them the well known systems where weak ferromagnetism was first analysed: $\alpha\text{-Fe}_2\text{O}_3$ (#0.66; Hill *et al.*, 2008), MnCO_3 (#0.115; Brown & Forsyth, 1967), CoCO_3 (#0.114; Brown *et al.*, 1973), NiCO_3 (#0.113; Plumier *et al.*, 1983) and FeBO_3 (#0.112; Pernet *et al.*, 1970). This large set of structures also includes ferrimagnetic structures, which have more than one symmetry-independent magnetic site, and have their easy axis along an FM direction of the MSG. In principle, weak ferromagnetism can be expected to be especially favourable if the symmetry-allowed FM mode belongs to the same irrep as the primary

Table 7

Non-polar magnetic phases in *MAGNDATA* with a transition temperature above 80 K which allow linear magnetoelectric properties if non-metallic.

Magnetoelectrics that support nonzero electric polarization at zero field are excluded by the non-polar condition on the MSG. Compounds that, to our knowledge, are metallic have also been excluded from the list.

Compound	Reference†	Parent space group	Magnetic space group‡	Magnetic point group	<i>T</i> (K)§
FePO ₄ (#0.17)	(a)	<i>Pnma</i>	<i>P2</i> ₁ 2 ₁ 2 ₁ (No. 19.25) ($\mathbf{a}_p, \mathbf{b}_p, \mathbf{c}_p; 0, \frac{1}{2}, \frac{3}{4}$)	222	125
Cr ₂ O ₃ (#0.59)	(b)	<i>R</i> ₃ <i>c</i>	<i>R</i> ₃ <i>c'</i> (No. 167.106) ($\mathbf{a}_p, \mathbf{b}_p, \mathbf{c}_p; 0, 0, 0$)	$\bar{3}'m'$	343
Cr ₂ TeO ₆ (#0.76; #0.143)	(c), (d)	<i>P</i> ₄ / <i>mnm</i>	<i>Pn</i> ' <i>nm</i> (No. 58.395) ($\mathbf{a}_p, \mathbf{b}_p, \mathbf{c}_p; \frac{1}{2}, \frac{1}{2}, \frac{1}{2}$)	<i>m'mm</i>	93
BaMn ₂ Bi ₂ (#0.89)	(e)	<i>I</i> ₄ / <i>m'm'm</i>	<i>I</i> ₄ '/ <i>m'm'm</i> (No. 139.536) ($\mathbf{a}_p, \mathbf{b}_p, \mathbf{c}_p; 0, 0, 0$)	<i>4'/m'm'm</i>	390
CaMn ₂ Sb ₂ (#0.92)	(f)	<i>P</i> ₃ <i>m</i> 1	<i>C</i> ₂ '/ <i>m</i> (No. 12.60) ($\mathbf{a}_p + 2\mathbf{b}_p, -\mathbf{a}_p, \mathbf{c}_p; 0, 0, 0$)	<i>2'/m</i>	83
Cr ₂ O ₃ (#0.110)	(g)	<i>R</i> ₃ <i>c</i>	<i>C</i> ₂ '/ <i>c</i> (No. 15.87) ($\frac{1}{3}\mathbf{a}_p + \frac{2}{3}\mathbf{b}_p - \frac{1}{3}\mathbf{c}_p, \mathbf{a}_p, -\frac{1}{3}\mathbf{a}_p - \frac{2}{3}\mathbf{b}_p + \frac{1}{3}\mathbf{c}_p; 0, \frac{1}{2}, 0$)	<i>2'/m</i>	308
MnGeO ₃ (#0.125)	(h)	<i>R</i> ₃	<i>R</i> ₃ ' (No. 148.19) ($\mathbf{a}_p, \mathbf{b}_p, \mathbf{c}_p; 0, 0, 0$)	$\bar{3}'$	120
Fe ₂ TeO ₆ (#0.142)	(i)	<i>P</i> ₄ / <i>mnm</i>	<i>P</i> ₄ ₂ / <i>m'n'm'</i> (No. 136.503) ($\mathbf{a}_p, \mathbf{b}_p, \mathbf{c}_p; 0, 0, 0$)	<i>4/m'm'm'</i>	219

† References: (a) Rousse *et al.* (2003), (b) Brown *et al.* (2002), (c) Zhu *et al.* (2014), (d) Kunmann *et al.* (1968), (e) Calder *et al.* (2014), (f) Ratcliff *et al.* (2009), (g) Fiebig *et al.* (1996), (h) Tsuzuki *et al.* (1974), (i) Kunmann *et al.* (1968). ‡ For the magnetic space group, the transformation to its standard setting from the parent basis is indicated. § Transition temperature.

AFM order parameter, and therefore can be linearly coupled with it, as happens in the classical weak ferromagnets mentioned above. The identification of the primary irrep and its equality or not with that of the FM mode(s) can easily be derived from the information available in *MAGNDATA* on the irrep decomposition of each structure. In any case, the large number of structures fulfilling the necessary symmetry conditions shows that weak ferromagnetism can be a rather common phenomenon, and it can be foreseen if the MSG of the structure is identified.

6.9. Multiferroics

Structures with polar symmetry and with their polarity being induced by the magnetic ordering can easily be retrieved from the collection, by looking for entries with a polar point group and a non-polar one for the parent phase. There are about 40 entries with this property, and those that are insulators fulfil the symmetry condition for being type II multiferroics. They are bound to have some magnetically induced electric polarization (whatever its size) with switching properties coupled with the magnetic order parameter. Many of them are well known multiferroics, but the possible ferroelectric character of a few additional ones has been shown for the first time through the symmetry assignment done in this database. A detailed discussion of these materials is the subject of a separate article (Perez-Mato *et al.*, 2016).

6.10. Magnetoelectrics

There are 56 non-polar structures that have an MSG which forbids zero-field electric polarization but allows linear magnetoelectricity in the case of insulators. Only 14 of them have a transition above 80 K, and this is reduced further to eight if compounds with known metallic properties are excluded. These eight structures are listed in Table 7. The publications where these structures were reported do not mention their potential magnetoelectricity, with the exception of the well known cases of Cr₂O₃ and Fe₂TeO₆.

6.11. Ferrotoroidics

In recent years, magnetic structures with spin arrangements possessing a nonzero toroidal moment have become the

subject of special attention (Schmid, 2001; Spaldin *et al.*, 2008; Ederer & Spaldin, 2007). The development of a spontaneous nonzero toroidal moment, being odd for time reversal and space inversion, is considered a fourth primary ferroic order, the so-called ferrotoroidicity, to be added to the traditional ferromagnetism, ferroelectricity and ferroelasticity. The possible presence of a nonzero toroidal moment in a magnetic structure is restricted by its point group symmetry. The number of magnetic point groups allowing a nonzero macroscopic toroidal moment is quite limited, namely 31 from the 122 possible magnetic point groups. About 60 structures, *i.e.* 15%, have one of these favourable symmetries. If one restricts the sample further to magnetic phases where the symmetry break is such that the primary magnetic order parameter describing the symmetry break has the properties of a toroidal moment, this number is further reduced. Table 8 lists the 29 structures from this set that do not allow electric polarization and/or macroscopic magnetization and can thus be denoted ‘pure’ ferrotoroidic. All possible orientational domains of these structures have a different orientation for the allowed toroidal moment, and the magnetic order parameter is linearly coupled with the so-called toroidal field ($\mathbf{H} \times \mathbf{E}$). Domain switching in these systems could in principle be possible with a combined application of magnetic and electric fields.

6.12. Contrast with macroscopic properties

Consistency with observed macroscopic properties can be a stringent test for a magnetic structure, and some of the models collected here are clearly inconsistent from this viewpoint. For instance, this is the case for LuFe₂O₄ (#1.0.7; Christianson *et al.*, 2008), which is claimed to be multiferroic, although the symmetry of the reported structure is incompatible with spin-driven or intrinsic ferroelectric properties. Something similar happens with the model of Cu₃Mo₂O₉ (#1.129; Vilminot *et al.*, 2009). Its 2'2'2' point group symmetry would not allow the ferroelectricity and weak ferromagnetism along **a** or **c** that is reported in other work (Hamasaki *et al.*, 2008; Hase *et al.*, 2015). Analogous situations were detected in other structures like DyVO₃ (#0.106; Reehuis *et al.*, 2011), Co₃TeO₆ (#0.145 and #1.164; Ivanov *et al.*, 2012) etc. In all such cases, the consistency problem is briefly indicated in the comments.

Table 8

Magnetic structures in *MAGNDATA* that can be classified as ‘pure’ ferrotoroidic phases, with their magnetic order parameter having the transformation properties of a toroidal moment, and the presence of a spontaneous electric polarization and/or macroscopic magnetization being symmetry forbidden.

Compound	Reference†	Parent space group	Magnetic space group‡	Magnetic point group
U ₃ Ru ₄ Al ₁₂ (#0.12)	(a)	P6/mmc	Cmcm' (No. 63.461) ($\mathbf{b}_p, -2\mathbf{a}_p - \mathbf{b}_p, \mathbf{c}_p; 0, 0, 0$)	m'mm
Gd ₅ Ge ₄ (#0.14)	(b)	Pnma	Pnm'a (No. 62.444) ($\mathbf{a}_p, \mathbf{b}_p, \mathbf{c}_p; 0, 0, 0$)	m'mm
EuTiO ₃ (#0.16)	(c)	I4/mcm	Fm'mmm (No. 69.523) ($\mathbf{a}_p - \mathbf{b}_p, \mathbf{a}_p + \mathbf{b}_p, \mathbf{c}_p; 0, \frac{1}{2}, \frac{1}{2}$)	m'mm
MnTiO ₃ (#0.19)	(d)	R̄3	R̄3' (No. 148.19) ($\mathbf{a}_p, \mathbf{b}_p, \mathbf{c}_p; 0, 0, 0$)	3'
DyB ₄ (#0.22)	(e)	P4/mbm	Pb'am (No. 55.355) ($\mathbf{b}_p, -\mathbf{a}_p, \mathbf{c}_p; 0, 0, 0$)	m'mm
LiFeSi ₂ O ₆ (#0.28)	(f)	P2 ₁ /c	P2 ₁ c' (No. 14.78) ($\mathbf{a}_p, \mathbf{b}_p, \mathbf{c}_p; 0, 0, 0$)	2/m'
Rb _y Fe _{2-x} Se ₂ (#0.54)	(g)	I4/m	I4/m' (No. 87.78) ($\mathbf{a}_p, \mathbf{b}_p, \mathbf{c}_p; 0, 0, 0$)	4/m'
K _y Fe _{2-x} Se ₂ (#0.55)	(h)	I4/m	I4/m' (No. 87.78) ($\mathbf{a}_p, \mathbf{b}_p, \mathbf{c}_p; 0, 0, 0$)	4/m'
Cr ₂ WO ₆ (#0.75)	(i)	P4 ₂ /mnm	Pn'nm (No. 58.395) ($\mathbf{b}_p, -\mathbf{a}_p, \mathbf{c}_p; 0, 0, 0$)	m'mm
Cr ₂ TeO ₆ (#0.76)	(j)	P4 ₂ /mnm	Pn'nm (No. 58.395) ($\mathbf{a}_p, \mathbf{b}_p, \mathbf{c}_p; \frac{1}{2}, \frac{1}{2}, \frac{1}{2}$)	m'mm
KMn ₄ (PO ₄) ₃ (#0.86)	(j)	Pnam	Pnma' (No. 62.445) ($\mathbf{a}_p, \mathbf{c}_p, -\mathbf{b}_p; 0, 0, 0$)	m'mm
NaFePO ₄ (#0.87)	(k)	Pnma	Pnma' (No. 62.445) ($\mathbf{a}_p, \mathbf{b}_p, \mathbf{c}_p; 0, 0, 0$)	m'mm
LiNiPO ₄ (#0.88)	(l)	Pnma	Pnm'a (No. 62.444) ($\mathbf{a}_p, \mathbf{b}_p, \mathbf{c}_p; 0, 0, 0$)	m'mm
CaMn ₂ Sh ₂ (#0.92)	(m)	P̄3m1	C2'/m (No. 12.60) ($\mathbf{a}_p + 2\mathbf{b}_p, -\mathbf{a}_p, \mathbf{c}_p; 0, 0, 0$)	2/m
LiFePO ₄ (#0.95)	(n)	Pnma	Pnma' (No. 62.445) ($\mathbf{a}_p, \mathbf{b}_p, \mathbf{c}_p; 0, 0, 0$)	m'mm
Cr ₂ O ₃ (#0.110)	(o)	R̄3c	C2'/c (No. 15.87) ($\frac{1}{3}\mathbf{a} + \frac{2}{3}\mathbf{b} - \frac{1}{3}\mathbf{c}, \mathbf{a} - \frac{1}{3}\mathbf{a} - \frac{2}{3}\mathbf{b} + \frac{1}{3}\mathbf{c}; 0, \frac{1}{2}, 0$)	2/m'
CoSe ₂ O ₅ (#0.119)	(p)	Pbcn	Pb'cn (No. 60.419) ($\mathbf{a}_p, \mathbf{b}_p, \mathbf{c}_p; 0, 0, 0$)	m'mm
MnGeO ₃ (#0.125)	(q)	R̄3	R̄3' (No. 148.19) ($\mathbf{a}_p, \mathbf{b}_p, \mathbf{c}_p; 0, 0, 0$)	3'
TbGe ₂ (#0.141)	(r)	Cnmmm	Cm'mm (No. 65.483) ($\mathbf{a}_p, \mathbf{b}_p, \mathbf{c}_p; 0, 0, 0$)	m'mm
Cr ₂ TeO ₆ (#0.143)	(s)	P4 ₂ /mnm	Pn'nm (No. 58.395) ($\mathbf{b}_p, -\mathbf{a}_p, \mathbf{c}_p; 0, 0, 0$)	m'mm
Cr ₂ WO ₆ (#0.144)	(s)	P4 ₂ /mnm	Pn'nm (No. 58.395) ($\mathbf{b}_p, -\mathbf{a}_p, \mathbf{c}_p; 0, 0, 0$)	m'mm
Co ₃ TeO ₆ (#0.145)	(t)	C2/c	C2'/c (No. 15.87) ($\mathbf{a}_p, \mathbf{b}_p, \mathbf{c}_p; 0, 0, 0$)	2/m'
EuZrO ₃ (#0.146)	(u)	Pnma	Pnm'a (No. 62.444) ($\mathbf{a}_p, \mathbf{b}_p, \mathbf{c}_p; 0, 0, 0$)	m'mm
LiFePO ₄ (#0.152)	(v)	Pnma	P2 ₁ c' (No. 14.78) ($-\mathbf{b}_p, -\mathbf{c}_p, \mathbf{a}_p; 0, 0, 0$)	2/m'
CaMnGe ₂ O ₆ (#0.156)	(w)	C2/c	C2'/c (No. 15.87) ($\mathbf{a}_p, \mathbf{b}_p, \mathbf{c}_p; 0, 0, 0$)	2/m'
TbCoO ₃ (#0.160)	(x)	Pbnm	Pnm'a (No. 62.444) ($-\mathbf{b}_p, \mathbf{c}_p, -\mathbf{a}_p; 0, 0, 0$)	m'mm
CoSe ₂ O ₅ (#0.161)	(y)	Pbcn	Pb'cn (No. 60.419) ($\mathbf{a}_p, \mathbf{b}_p, \mathbf{c}_p; 0, 0, 0$)	m'mm
NdCrTiO ₅ (#0.162)	(z)	Pbam	Pbam' (No. 55.356) ($\mathbf{a}_p, \mathbf{b}_p, \mathbf{c}_p; 0, 0, 0$)	m'mm
MnPS ₃ (#0.163)	(aa)	C2/m	C2'/m (No. 12.60) ($\mathbf{a}_p, \mathbf{b}_p, \mathbf{c}_p; 0, 0, 0$)	2/m'

† References: (a) Troć *et al.* (2012), (b) Tan *et al.* (2005), (c) Scagnoli *et al.* (2012), (d) Shirane *et al.* (1959), (e) Will & Schafer (1979), (f) Redhammer *et al.* (2009), (g) Pomjakushin *et al.* (2011), (h) Pomjakushin *et al.* (2011), (i) Zhu *et al.* (2014), (j) López *et al.* (2008), (k) Avdeev *et al.* (2013), (l) Jensen *et al.* (2009), (m) Ratcliff *et al.* (2009), (n) Rousse *et al.* (2003), (o) Fiebig *et al.* (1996), (p) Melot *et al.* (2010), (q) Tsuzuki *et al.* (1974), (r) Schobinger-Papamantellos *et al.* (1988), (s) Kunmann *et al.* (1968), (t) Ivanov *et al.* (2012), (u) Avdeev *et al.* (2014), (v) Toft-Petersen *et al.* (2015), (w) Ding *et al.* (2016), (x) Knížek *et al.* (2014), (y) Rodriguez *et al.* (2016), (z) Buisson (1970), (aa) Ressouche *et al.* (2010). ‡ For the magnetic space group, the transformation to its standard setting from the parent basis is indicated.

6.13. Secondary modes: higher harmonics

The MSG of about 10% of the structures allows the presence of secondary irreducible spin modes, *i.e.* spin modes transforming according to an irrep which is not that of the order parameter. These spin modes are not necessary for the symmetry break, but they are symmetry allowed and may be present in the structure as a secondary induced effect. These secondary irreducible spin distortions, which are expected to be very weak, remain unobserved in most cases, but one must take into account that the traditional representation method used in the refinements, which only considers possible models subject to a single irrep, implies their *a priori* exclusion. In any case, structures with MSGs that allow secondary modes are those where a combined application of the constraints coming from the relevant MSG and from the assumption of a single primary irrep is most convenient, in order to reduce the number of degrees of freedom with respect to the sole application of the MSG symmetry relations.

It is remarkable that secondary modes, generally absent, have large amplitudes in structures where they have been forced *a priori* in the refined model. For instance, this is the case for structures that allow secondary modes corresponding to higher harmonics of the propagation vector, *i.e.* cases where $3\mathbf{k}$ is not equivalent to \mathbf{k} . The 11 structures classified with the labels 1.0.xxx in *MAGNDATA* are all of this type. Many of

these structures are modelled assuming collinear spin arrangements, where the spin modulus and orientation are maintained at all sites and only its direction can switch sign.

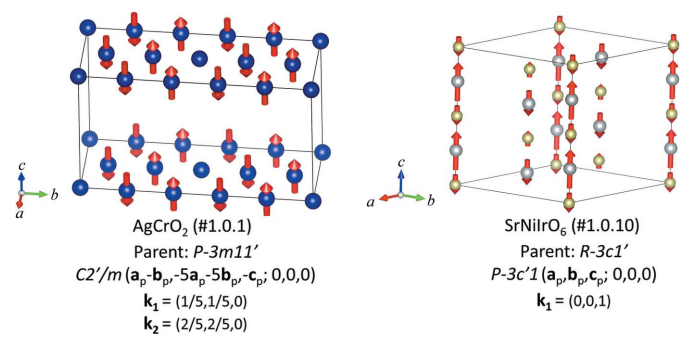


Figure 15

Single- \mathbf{k} magnetic structures of AgCrO₂ (Matsuda *et al.*, 2012) and SrNilrO₆ (Lefrançois *et al.*, 2014) as examples of the two different approaches when dealing with structures with propagation vectors and symmetries that allow the presence of secondary modes in the form of spin wave harmonics. In the first structure, the harmonic with propagation vector $3\mathbf{k}$ is necessarily present in the model to produce equality of all spin moduli, while in the second one, a sinusoidal spin wave according to the primary propagation vector is proposed and the symmetry-allowed $3\mathbf{k}$ ($= 0$) component is absent. In both cases, no experimental evidence of a third harmonic seems to exist. Below each structure, the parent grey space group, the MSG and the modulation wavevectors present in the structure are indicated.

These spin arrangements do not fulfil the usual single-irrep assumption and require significant nonzero amplitudes of higher harmonics of the primary spin mode. Magnetic Bragg peaks for odd multiples of the propagation vector should be present in the diffraction diagram, but often these simplified models are assumed without experimental evidence for higher harmonics in the spin wave. The equality of the spin modulus at all sites is generally considered physically more appealing than the single-irrep assumption, which would imply a sinusoidal spin wave. However, one can find both types of approach in the proposed models in the literature. Fig. 15 shows two examples.

6.14. Secondary modes with the primary propagation vector

From the approximately 30 structures with MSGs that allow the presence of secondary modes with the same propagation vector as the primary spin arrangement, there are only six where the amplitude of these secondary degrees of freedom is nonzero. The case of $\text{Er}_2\text{Ru}_2\text{O}_7$ (#0.154; Taira *et al.*, 2003) is an interesting example. Its MSG is $I4_1'/am'd$, i.e. it is one of the maximal epikernels of the irrep $m\text{GM}3+$ (see §5 and Fig. 10). Fig. 16 shows the reported structure of this compound compared with that of $\text{Er}_2\text{Ti}_2\text{O}_7$ (#0.29; Poole *et al.*, 2007). While the spin arrangement in $\text{Er}_2\text{Ti}_2\text{O}_7$ has been modelled assuming the presence of only the primary irrep $m\text{GM}3+$, and therefore the symmetry-allowed secondary spin mode according to irrep $m\text{GM}2+$ is absent, the spin ordering in $\text{Er}_2\text{Ru}_2\text{O}_7$ has been refined as a collinear arrangement. The simplicity of this second model hides a rather exceptional behaviour when seen in terms of irreps. The collinearity does not imply an MSG different from that of $\text{Er}_2\text{Ti}_2\text{O}_7$, but it requires the presence of a spin mode according to the

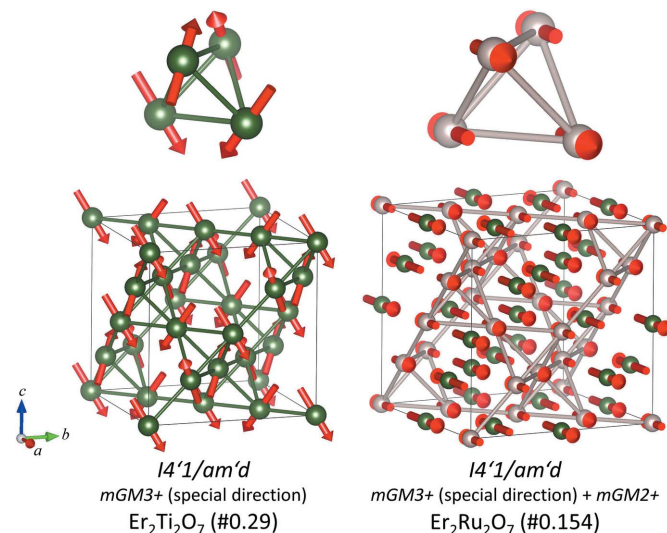


Figure 16

Two magnetic structures complying with the same MSG $I4_1'/am'd$. The structure reported for $\text{Er}_2\text{Ti}_2\text{O}_7$ (Poole *et al.*, 2007) includes a single spin mode with two-dimensional $m\text{GM}3+$ irrep basis functions specialized to this MSG, while the collinear model of $\text{Er}_2\text{Ru}_2\text{O}_7$ (Taira *et al.*, 2003) requires the additional presence of a secondary $m\text{GM}2+$ mode compatible with the same MSG.

secondary irrep $m\text{GM}2+$, and with a large specific amplitude correlated with that of the primary active irrep. From the original publication, it is not clear if this rather unusual weight of a secondary irrep mode is the result of an *a priori* collinearity assumption, or whether it was contrasted with a pure $m\text{GM}3+$ model, being then fully supported by the experimental data. The presence of secondary irrep modes of this type in four of the six structures can be traced back to such types of assumption or extrinsic conditions. This is the case for Mn_3GaC (#1.153; Fruchart *et al.*, 1970), where collinearity also forces the presence of a secondary irrep mode, $\text{U}_3\text{Ru}_4\text{Al}_{12}$ (#0.12; Troć *et al.*, 2012), where some specific relative spin orientations not forced by symmetry are included in the model, and $\text{Tb}_2\text{Ti}_2\text{O}_7$ (#0.77; Sazonov *et al.*, 2013), which is a structure stabilized by an external magnetic field.

Therefore, only two structures in the whole collection include a significant contribution of a secondary irrep mode that was independently monitored and did not originate from some assumption. These are the structures of Cr_2S_3 (#0.5; Bertaut *et al.*, 1968) and $\text{Nd}_3\text{Ru}_4\text{Al}_{12}$ (#0.149; Gorbunov *et al.*, 2016). In both cases, the amplitudes of both primary and secondary modes are comparable, and therefore it does not seem appropriate to consider one of them as an induced secondary effect. Despite the symmetry compatibility of one of the modes with respect to the other, it seems that, in these two cases, one should consider the two spin components as ordering modes associated with two independent primary order parameters.

6.15. Multi- \mathbf{k} structures

Reported magnetic structures with more than one propagation vector are scarce. Despite our efforts to find well defined experimental structures in the literature with several independent propagation vectors, the numbers of $2\mathbf{k}$ and $3\mathbf{k}$ structures that we could collect were only 15 and eight, respectively. These include structures with symmetry-related propagation vectors. Only six $2\mathbf{k}$ structures have a parent symmetry relating the two active propagation vectors, while in the case of the $3\mathbf{k}$ structures, seven of the eight involve three primary propagation vectors related by the parent symmetry, either cubic or hexagonal. Fig. 17 shows some examples.

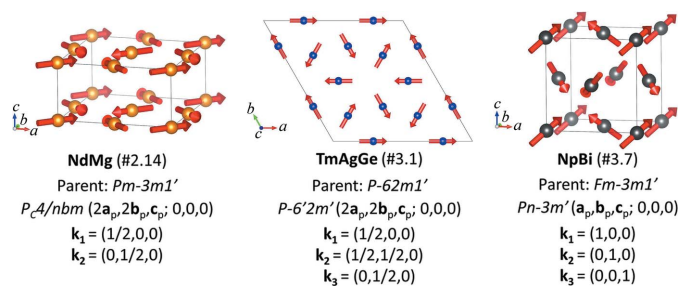


Figure 17

The magnetic structures of NdMg (Deldem *et al.*, 1998), TmAgGe (Baran *et al.*, 2009) and NpBi (Burlet *et al.*, 1992) as examples of multi- \mathbf{k} structures with symmetry-related propagation vectors. Below each figure, the parent grey space group, the MSG of the phase and the active independent propagation vectors with respect to the parent structure are indicated.

It must be stressed that the magnetic symmetry of a commensurate multi- \mathbf{k} structure is also given by an MSG, having from this viewpoint no essential difference from a single- \mathbf{k} structure. The number of independent propagation vectors associated with the spin modulation comes from a comparison with the parent paramagnetic structure, and it is not an intrinsic property of the spin arrangement. The magnetic structure is fully defined by its relevant MSG, its unit cell, and the set of atomic positions and magnetic moments of its asymmetric unit, without any reference to the underlying propagation vectors with respect to the parent structure. For instance, the magnetic structure of NpBi (#3.7; Burlet *et al.*, 1992) represented in Fig. 17 has a parent phase with space group $Fm\bar{3}m$. The magnetic ordering breaks all the centring translations while keeping the cubic unit cell and results in the MSG $Pn\bar{3}m'$. This can be described by the condensation of spin waves with the propagation vectors $(1, 0, 0)$, $(0, 1, 0)$ and $(0, 0, 1)$ on the reference paramagnetic face-centred cubic structure. However, the same spin arrangement for the same magnetic sites and with the same MSG can be realized in a magnetic phase having a parent structure with a primitive cubic lattice and space group $Pn\bar{3}m'$. In such a case, the same spin arrangement would be described as a single- \mathbf{k} magnetic structure with $\mathbf{k} = 0$.

Multi- \mathbf{k} structures with symmetry-related \mathbf{k} vectors are in general indistinguishable from single- \mathbf{k} structures in powder diffraction experiments. Even in the case of single-crystal studies, the distinction between a multi- \mathbf{k} and a single- \mathbf{k} structure with appropriate domain populations can be problematic. Most of the collected multi- \mathbf{k} structures with symmetry-related \mathbf{k} vectors correspond to single-crystal studies, but not all [see, for instance, TmAgGe (#3.1; Baran *et al.*, 2009)]. It is generally believed that the diffraction diagrams of single- \mathbf{k} structures should change considerably under an external magnetic field owing to changes in the domain populations, while those of multi- \mathbf{k} structures should be rather insensitive. Under this assumption, the study of the variation in a single-crystal diffraction diagram under a magnetic field has become a traditional form of identifying multi- \mathbf{k} spin arrangements, and was used in the studies of some of the structures collected here.

More than 50 single- \mathbf{k} structures in this collection have a propagation vector and a parent symmetry such that alternative multi- \mathbf{k} models would be possible. In most cases, these multi- \mathbf{k} models have not been explored as possible alternative models. Usually when confronted with this problem, the single- \mathbf{k} model is preferred *a priori* and it is the one reported. One should be aware, however, that multi- \mathbf{k} models could equally well fit the experimental data in most such cases. If an alternative multi- \mathbf{k} model has also been reported, both have been included in the collection, but this situation rarely happens.

6.16. Multi-axial structures

Sometimes the so-called multi-axial structures, where the spins orientate according to several different fixed directions,

are assimilated with the multi- \mathbf{k} structures. However, multi-axial spin arrangements are not exclusive to multi- \mathbf{k} structures and they can also be a symmetry-protected feature of single- \mathbf{k} structures. Fig. 18 shows some examples where multiple axes for the spin orientations are symmetry dictated and a single propagation vector exists with respect to the parent phase.

6.17. Conflicting models

MAGNDATA has more than one magnetic structure for around 50 compounds. In most cases they correspond to different magnetic phases or to the same phase under a different temperature, field *etc*. In other cases they correspond to a different model for the same phase reported by different authors, and the structures are very similar. In a few cases they represent several alternative indistinguishable models that have been reported in the same reference. But in the case of 12 compounds, and for apparently the same phase, this collection has gathered magnetic structures that differ by a significant amount. They are summarized in Table 9.

In EuZrO_3 (Avdeev *et al.*, 2014; Saha *et al.*, 2016), one finds a typical case where the easy axis of a collinear arrangement seems difficult to establish and two different studies report different directions. But, depending on this direction, the relevant MSG changes, and this dictates different magneto-structural properties, like the allowance or not of linear magnetoelectric (ME) effects. Through the direct link to the program *MAGNEXT*, one can also see that the two models imply different systematic absences in the diffraction diagram, which could in principle help to differentiate between the two

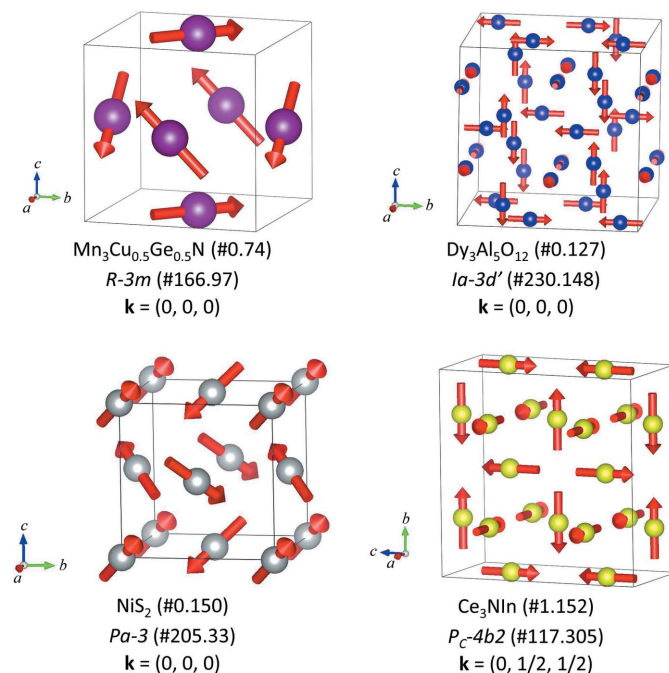


Figure 18

The magnetic structures of $\text{Mn}_3\text{Cu}_{0.5}\text{Ge}_{0.5}\text{N}$ (Iikubo *et al.*, 2008), $\text{Dy}_3\text{Al}_5\text{O}_{12}$ (Hastings *et al.*, 1965), NiS_2 (Yano *et al.*, 2016) and Ce_3NiIn (Gäbler *et al.*, 2008) as examples of multi-axial structures with a single propagation vector. Below each figure, the label of the corresponding MSG and the propagation vector are indicated.

Table 9

Conflicting structures for the same magnetic phase in MAGNDATA.

In the column headed ‘Experimental technique’, NPD denotes neutron powder diffraction and NSD denotes neutron single-crystal diffraction. In the column headed ‘SA’, a cross (×) indicates that the systematic absences are different for the two proposed models.

Compound	Entries	Reference†	Parent space group	Magnetic space group	Comparison	Experimental technique	SA
BiMn ₂ O ₅	1.74	(a)	<i>Pbam</i>	<i>C₄mc2</i> ₁	Same irrep	NPD	
	1.75	(b)		<i>C₄m</i>	Group–subgroup relation		NSD
CaMnGe ₂ O ₆	0.156	(c)	<i>C2/c</i>	<i>C₂'/c</i>	One-irrep model	NPD	
	0.155	(d)		<i>P_s1'</i>	Two-irrep model		NPD
CoSe ₂ O ₅	0.119	(e)	<i>Pbcn</i>	<i>Pb'cn</i>	Same irrep	NPD	
	0.161	(f)			With and without spin canting		NSD
Cu ₃ Mo ₂ O ₉	0.129	(g)	<i>Pnma</i>	<i>P2₁2₁2₁</i>	Two irreps, one equal and the other different	NPD	
	0.130	(h)		<i>Pm'c2</i> ₁			NSD
EuZrO ₃	0.146	(i)	<i>Pnma</i>	<i>Pnm'a</i>	Different easy axis	NPD	
	0.147	(j)		<i>Pn'm'a</i>	Different single irrep, ME effect allowed in one of the models		NSD
Gd ₂ CuO ₄	0.82	(k)	<i>Aeam</i>	<i>Cm'ca'</i>	Different parent symmetry	NSD	
	0.104	(l)		<i>I4/mmm</i>	Inclusion or not of a structural distortion		NSD
HoMnO ₃	0.33	(m)	<i>P6₃cm</i>	<i>P6₃cm</i>	Different single irrep	NPD	
	0.43	(n)		<i>P6₃cm'</i>			NSD
LiFePO ₄	0.95	(o)	<i>Pnma</i>	<i>Pnma'</i>	One-irrep and two-irrep models; second irrep: small spin canting that breaks the symmetry	NPD	
	0.152	(p)		<i>P2₁/c'</i>	Group–subgroup relation		NSD
NiTa ₂ O ₆	1.112	(q)	<i>P4₂/mnm</i>	<i>P_c2₁/c</i>	Two irreps, one equal and the other different	NPD	
	1.172	(r)		<i>A₁ba2</i>			NSD
Sr ₂ IrO ₄	1.3	(s)	<i>I4₁/acd</i>	<i>P_ccca</i>	Same irrep, same symmetry	NPD	
	1.77	(t)			Without and with canting		NSD
YMnO ₃	0.6	(u)	<i>P6₃cm</i>	<i>P6₃cm</i>	One-irrep and two-irrep models	NPD	
	0.44	(v)		<i>P6</i> ₃	No common irrep		NSD
La _{0.333} Ca _{0.667} MnO ₃	1.174	(w)	<i>Pnma</i>	<i>P_bmc2</i> ₁	Different parent structure, different orientation of the propagation vector	NPD	
	1.175			<i>P_bmn2</i> ₁			NSD

† References: (a) Muñoz *et al.* (2002), (b) Vecchini *et al.* (2008), (c) Ding *et al.* (2016), (d) Redhammer *et al.* (2008), (e) Melot *et al.* (2010), (f) Rodriguez *et al.* (2016), (g) Vilminot *et al.* (2009), (h) Hase *et al.* (2015), (i) Avdeev *et al.* (2014), (j) Saha *et al.* (2016), (k) Brown & Chatterji (2011), (l) Chattopadhyay *et al.* (1992), (m) Muñoz, Alonso *et al.* (2001), (n) Brown & Chatterji (2006), (o) Rousse *et al.* (2003), (p) Toft-Petersen *et al.* (2015), (q) Law *et al.* (2014), (r) Ehrenberg *et al.* (1998), (s) Lovesey *et al.* (2012), (t) Ye *et al.* (2013), (u) Muñoz *et al.* (2000), (v) Radaelli *et al.* (1999), (w) Fernández-Díaz *et al.* (1999).

models. There are also cases where the two models have the same symmetry, and the difference is the presence or not of a significant spin canting fully compatible with the MSG of the structure. We have already mentioned the case of CoSe₂O₅ (Melot *et al.*, 2010; Rodriguez *et al.*, 2016), and something similar happens for Sr₂IrO₄ (Lovesey *et al.*, 2012; Ye *et al.*, 2013).

The cases of BiMn₂O₅ (Vecchini *et al.*, 2008; Muñoz *et al.*, 2002), already discussed above, and LiFePO₄ (Rousse *et al.*, 2003; Toft-Petersen *et al.*, 2015) are representative of situations where the structural models differ only slightly, but this difference breaks the symmetry further, therefore implying an important qualitative difference. In one case it reduces the MSG of the structure to the kernel of the irrep, and in the other it implies the activity of a second primary irrep with a very weak amplitude. A detailed comparison of the two models of the magnetic structure of BiMn₂O₅ can be seen in Table 10. One can observe that the deviations of the low-symmetry model from one of higher symmetry are close to their standard deviations, which would imply that the system complies with one of the maximal epikernels of the active irrep. However, apart from the larger magnetic moments of the high-symmetry model, one can see that the spin canting components along **b** for the Mn2 sites have opposite signs in the two structures. It can also be noted that the model of higher symmetry, apart from the moment relations consistent

with the indicated irrep epikernel, includes some additional constraints that are not symmetry-forced. Its asymmetric unit has three Mn sites, namely Mn1_1, and two independent sites Mn2_1 and Mn2_2, which are the result of the splitting of the single Mn2 site in the parent *Pbam* symmetry. The model reported by Muñoz *et al.* (2002) includes some specific correlation between the components of these two independent sites and has the allowed z component of Mn1_1 fixed to zero, but the structure has only a single irrep active and its symmetry is maximal. Therefore, these additional constraints are not justified by either the assumption of a specific irrep spin mode or any other symmetry argument, and they could have been skipped, even if they are fulfilled approximately. This is an example of overconstraints in the structure modelling, an issue discussed below in more detail.

The remaining pairs of structures summarized in Table 9 correspond to models which differ in a higher degree: they have no group–subgroup-related MSGs, different active irreps etc. For instance, Fig. 19 shows the two very different magnetic structures proposed for Cu₃Mo₂O₉ (Vilminot *et al.*, 2009; Hase *et al.*, 2015). The case of La_{0.333}Ca_{0.667}MnO₃ (Radaelli *et al.*, 1999; Fernández-Díaz *et al.*, 1999) is also remarkable. Although the spin arrangements of the two models are very similar, their orientation relative to the parent structure is completely different, both structures having distinct MSGs. A small structural distortion of the parent structure is also

Table 10

Comparison of the magnetic structures #1.74 and #1.75, reported for BiMn_2O_5 by Muñoz *et al.* (2002) and Vecchini *et al.* (2008) at 1.5 and 10 K, respectively.

The MSG for each structure and the corresponding asymmetric unit for the Mn atoms are listed. The basis $(2\mathbf{a}_p, \mathbf{b}_p, 2\mathbf{c}_p; 0, 0, 0)$ with respect to the parent $Pbam$ unit cell is used for the description. Only approximate atomic positions are listed. In the case of the model with higher symmetry and smaller asymmetric unit, the spins of symmetry-related atoms are also included for comparison. Structure #1.74 has been transformed to the domain-related equivalent with all spins switched.

BiMn ₂ O ₅ (#1.75)												BiMn ₂ O ₅ (#1.74)						
Label	x	y	z	Pbam1' $\rightarrow C_d m$ ($2\mathbf{a}_p, -\mathbf{c}_p, 2\mathbf{b}_p; 0, 0, 0$)				Constraints†	M_x	M_y	M_z	\mathbf{M}	Pbam1' $\rightarrow C_d mc2_1$ ($2\mathbf{c}_p, \mathbf{a}_p, 2\mathbf{b}_p; \frac{1}{8}, 0, 0$)					
				Constraints†	M_x	M_y	M_z						Constraints†	M_x	M_y	M_z	\mathbf{M}	
Mn1_1	0.00	0.50	0.37	m_x, m_y, m_z	2.10 (3)	-0.33 (6)	-0.25 (6)	2.14	m_x, m_y, m_z	2.44 (10)	-0.6 (2)	0.0	2.51	m_x, m_y, m_z	2.44	0.6	0.0	2.51
Mn1_2	0.25	0.00	0.13	m_x, m_y, m_z	2.07 (3)	0.56 (6)	0.08 (6)	2.15	$m_x, -m_y, m_z$	2.44	0.6	0.0	2.51	$m_x, m_y, 0$	-3.12 (9)	-0.8 (2)	0.0	3.22
Mn2_1	0.20	0.35	0.25	$m_x, m_y, 0$	-2.83 (5)	0.33 (10)	0.0	2.85	$m_x, m_y, 0$	2.84	$m_x, -m_y, 0$	-3.12	0.8	$m_x, -m_y, 0$	3.12	0.8	0.0	3.22
Mn2_3	0.05	0.85	0.25	$m_x, m_y, 0$	-2.83 (5)	-0.23 (10)	0.0	2.84	$m_x, -m_y, 0$	-3.12	0.8	0.0	3.22	$-m_x, -m_y, 0$	3.12	0.8	0.0	3.22
Mn2_2	0.30	0.65	0.25	$m_x, m_y, 0$	2.80 (5)	-0.34 (9)	0.0	2.82	$-m_x, -m_y, 0$	2.81	$m_x, -m_y, 0$	-3.12	0.8	$m_x, -m_y, 0$	3.12	0.8	0.0	3.22
Mn2_4	0.45	0.15	0.25	$m_x, m_y, 0$	-2.74 (5)	-0.64 (10)	0.0	2.81	$m_x, -m_y, 0$	2.81	$m_x, -m_y, 0$	-3.12	0.8	$m_x, -m_y, 0$	3.12	0.8	0.0	3.22

† Symmetry constraints on the magnetic moment \mathbf{M} .

oriented differently in the two models. The tetragonal pseudo-symmetry of the parent structure, and especially of the Mn sites, seems to be the cause for these two very different models being able to fit the diffraction data reasonably well. A model very similar to the one reported by Radaelli *et al.* (1999) has recently been reported for a compound with a similar composition, $\text{La}_{0.375}\text{Ca}_{0.625}\text{MnO}_3$ (#1.173; Martinelli *et al.*, 2016).

6.18. ‘Concomitant’ structural transitions

About 60% of the collected structures have a magnetic ordering whose symmetry implies some symmetry break for the non-magnetic degrees of freedom. In other words, the MSG of the magnetic structure allows structural distortions forbidden in the parent space group, which can in principle become nonzero through magnetostructural coupling. These include of course the spin-driven multiferroics discussed above. In most cases, the structural distortions that are consistent with the MSG and break the parent space group are

too weak to be detected. As they are so rare, if they are detected such distortions are often erroneously considered as a so-called concomitant or simultaneous structural phase transition.

Table 11 summarizes the structures in the collection where such types of concomitant structural distortions have been reported. The effective space group relevant for the non-magnetic degrees of freedom is given by the space group used to label the MSG in the OG setting. Although this collection employs the BNS notation for the MSG labels, a link in the BNS label of the MSG of each entry allows the user to obtain the corresponding OG label and extract from it the effective space group that is relevant for the non-magnetic degrees of freedom. Table 11 indicates this effective space group for the 18 listed structures. The structural distortions of all compounds in Table 11 seem consistent with the corresponding effective space group, except for YFe_4Ge_2 and LuFe_4Ge_2 (Schobinger-Papamantellos *et al.*, 2001, 2012). In these two compounds, the reported simultaneous structural symmetry break $P4_2/mnm \rightarrow Pnnm$ cannot be explained as an induced effect of the reported spin arrangement, which without the conjunction of the structural distortion would have a higher MSG. Hence, these two compounds are the only cases in the collection where a genuine simultaneous independent structural phase transition takes place. One must be aware, however, that spin arrangements alternative to those reported could explain the symmetry break observed in these compounds in the non-magnetic structural degrees of freedom as an induced effect, and it seems they were not explored.

The symmetry-breaking structural distortions of the other 16 structures in Table 11 seem to comply with the expected symmetry constraints resulting from the MSG associated with the spin ordering. Some of them have been refined under the corresponding effective space group and are therefore fully consistent as an induced effect. In a couple of cases, the space group employed in the refinement of the positional structure is a supergroup of the effective space group, and therefore the observed structural distortion is also consistent with the MSG, but it was partially constrained by the assumed model. In some other cases, the structural distortion is observed and reported,

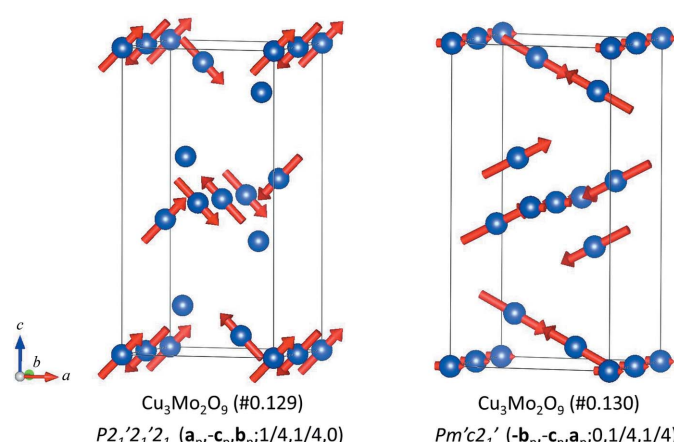


Figure 19
Conflicting magnetic structures for the same phase of $\text{Cu}_3\text{Mo}_2\text{O}_9$ (Vilminot *et al.*, 2009; Hase *et al.*, 2015), with indications of the MSGs and the transformation to the standard setting of each group from the parent $Pnma$ basis.

Table 11

Structures in *MAGNDATA* where a symmetry-breaking structural distortion is reported to be concomitant with the magnetic transition.

The column headed ‘Structural distortion’ indicates if the structural distortion is fully consistent as an induced effect (‘Present’), has been constrained *a priori* by the refined model (‘Present partially’), is reported in another reference (‘Other reference’), is reported but not characterized (‘Reported but not characterized’), or is inconsistent as an induced effect and must be considered an independent structural transition (‘Concomitant structural transition?’).

Entry	Reference [†]	k vector(s)	Parent space group	Magnetic space group	Effective space group [‡]	Structural distortion
BaFe ₂ As ₂ (#1.16)	(a)	($\frac{1}{2}$, $\frac{1}{2}$, 0)	<i>I</i> 4/mmm	<i>C</i> _{Amca} (No. 64.480)	<i>F</i> mmm	Present
CaFe ₂ As ₂ (#1.52)	(b)	($\frac{1}{2}$, $\frac{1}{2}$, 0)	<i>I</i> 4/mmm	<i>C</i> _{Amca} (No. 64.480)	<i>F</i> mmm	Present
CoO (#1.69)	(c)	($\frac{1}{2}$, $\frac{1}{2}$, $\frac{1}{2}$)	<i>Fm</i> $\bar{3}m$	<i>C</i> _{2/c} (No. 15.90)	<i>C</i> 2/m	Present
α -Mn (#1.85)	(d)	(1, 0, 0)	<i>I</i> $\bar{4}3m$	<i>P</i> _{$\bar{1}$} 42_1c (No. 114.282)	<i>I</i> $\bar{4}2m$ (No. 121)	Present
GeV ₄ S ₈ (#1.86)	(e)	($\frac{1}{2}$, $\frac{1}{2}$, 0)	<i>F</i> $\bar{4}3m$	<i>P</i> _{d} $na2_1$ (No. 33.149)	<i>Pmn2</i> ₁	Present
AgCrS ₂ (#1.136)	(f)	($-\frac{3}{4}$, $\frac{3}{4}$, $-\frac{3}{4}$)	<i>R</i> 3m	<i>C</i> _{\bar{m}} (No. 8.35)	<i>C</i> m	Present
MnCuO ₂ (#1.57)	(g)	($-\frac{1}{2}$, $\frac{1}{2}$, $\frac{1}{2}$)	<i>C</i> 2/m	<i>P</i> _{s} $\bar{1}$ (No. 2.7)	<i>P</i> $\bar{1}$	Present
Sr ₂ CoOsO ₆ (#1.72)	(h)	($\frac{1}{2}$, $\frac{1}{2}$, 0)	<i>I</i> 4/m	<i>C</i> _{2/c} (No. 15.90)	<i>C</i> 2/c	Present
Ag ₂ CrO ₂ (#1.0.1)	(i)	($\frac{1}{2}$, $\frac{1}{2}$, 0) ($\frac{2}{3}$, $\frac{2}{3}$, 0)	<i>P</i> $\bar{3}m$ 1	<i>C</i> 2'/m (No. 12.60)	<i>C</i> 2/m	Present partially
DyFe ₄ Ge ₂ (#1.98)	(j)	($\frac{1}{4}$, $\frac{1}{4}$, 0)	<i>P</i> 4/mnm	<i>P</i> _{c} c 2 (No. 27.82)	<i>Pmm2</i>	Present partially
NiF ₂ (#0.36)	(k)	(0, 0, 0)	<i>P</i> 4 ₂ /mnm	<i>Pnn'm'</i> (No. 58.398)	<i>Pnnm</i>	Other reference
ErVO ₃ (#0.104)	(l)	(0, 0, 0)	<i>Pbnm</i>	<i>P</i> 2 ₁ /m' (No. 11.54)	<i>P</i> 2 ₁ /m	Reported but not characterized
ErVO ₃ (#0.105)	(m)	(0, 0, 0)	<i>Pbnm</i>	<i>P</i> 2 ₁ /c (No. 14.75)	<i>P</i> 2 ₁ /c	Reported but not characterized
DyVO ₃ (#0.106)	(m)	(0, 0, 0)	<i>Pbnm</i>	<i>P</i> 2 ₁ /m' (No. 11.54)	<i>P</i> 2 ₁ /m	Reported but not characterized
BaFe ₂ Se ₃ (#1.120)	(n)	($\frac{1}{2}$, $\frac{1}{2}$, $\frac{1}{2}$)	<i>Pnma</i>	<i>C</i> _{ac} (No. 9.41)	<i>P</i> c	Reported but not characterized
Mn ₃ CuN (#2.5)	(o)	($\frac{1}{2}$, $\frac{1}{2}$, 0) (0,0,0)	<i>P</i> $\bar{m}\bar{3}m$	<i>P</i> 4/n (No. 85.59)	<i>P</i> 4/n	Reported but not characterized
YFe ₄ Ge ₂ (#0.27)	(p)	(0, 0, 0)	<i>P</i> 4 ₂ /mnm	<i>P</i> n'n'm' (No. 58.399)	<i>Pnnm</i>	Concomitant structural transition?
LuFe ₄ Ge ₂ (#0.140)	(q)	(0, 0, 0)	<i>P</i> 4 ₂ /mnm	<i>P</i> n'n'm' (No. 58.399)	<i>Pnnm</i>	Concomitant structural transition?

[†] References of the magnetic structures: (a) Huang *et al.* (2008), (b) Goldman *et al.* (2008), (c) Jauch *et al.* (2001), (d) Lawson *et al.* (1994), (e) Müller *et al.* (2006), (f) Damay *et al.* (2011), (g) Damay *et al.* (2009), (h) Yan *et al.* (2014), (i) Matsuda *et al.* (2012), (j) Schobinger-Papamantellos *et al.* (2006), (k) Brown & Forsyth (1981), (l) Chattopadhyay *et al.* (1992), (m) Reehuis *et al.* (2011), (n) Caron *et al.* (2011), (o) Fruchart & Bertaut (1978), (p) Schobinger-Papamantellos *et al.* (2001), (q) Schobinger-Papamantellos *et al.* (2012). [‡] For non-magnetic degrees of freedom.

but owing to its weakness it was not characterized and was not included in the magnetic structure.

6.19. Overconstrained structures

The description of magnetic structures in *MAGNDATA* using their MSG allows us to distinguish in the model, in a straightforward form, the constraints that are forced and protected by symmetry from those that are not. Constraints that are not symmetry dictated are very common, and they reduce the number of free parameters with respect to a general model complying with the relevant MSG. There can be good reasons for having a structure with fewer free parameters than those allowed by the associated magnetic symmetry, and some of them have already been discussed above. They can be summarized in the following points:

(i) Collinearity favoured by exchange-type interactions can prevail and strict collinearity can be assumed, despite the MSG allowing non-collinear spin canting. See, for instance, the case of ErAuGe (#1.33; Baran *et al.*, 2001).

(ii) If the magnetic structure has a single active irrep but the resulting MSG allows secondary magnetic irreps, the presence of these additional degrees of freedom is usually negligible and the model can be restricted to the primary irrep (constrained along the direction dictated by the MSG). See, for instance, the case of GdB₂Pt (#1.111; Müller *et al.*, 2014).

(iii) If several irreps are active, the resulting MSG usually has a very low symmetry. As a consequence, several additional secondary irreps may be symmetry allowed, but they correspond to very weak high-order effects. In such cases, the

restriction of the spin arrangement to the primary irreps implies a substantial reduction in the effective number of degrees of freedom. See, for instance, the case of CsNiCl₃ (#1.0.4; Yelon & Cox, 1973).

In the traditional representation method, restrictions on the possible combinations of basis spin modes corresponding to the active irrep (or irreps) are usually introduced through a mixture of *ad hoc* simplifications and/or intuitive assumptions combined with trial and error methods. This implies that, in general, the final model may include constraints that cannot be justified on symmetry or physical grounds. Thus, in complex structures the constraints corresponding to a particular irrep epikernel, or the three types of physical restriction mentioned above, are usually mixed up with others that can only be considered convenient simplifications to reduce the number of refinable parameters. An example has already been shown above when discussing the structure of BiMn₂O₅ (Muñoz *et al.*, 2002), summarized in Table 10. This kind of simplification is so common that it sometimes seems as if it is introduced automatically without being necessitated by the limitations of the experimental data.

One of the most common constraints not forced by symmetry and present in many structures of this database is the restriction of the modulus of the magnetic moment for the same atomic species to have equal value at sites that are symmetry independent in the paramagnetic phase. This *ad hoc* assumption can often represent a reasonable simplification and can be necessary owing to the lack of sufficient data for a more complex model but, in general, independent sites can have different magnetic moments and this collection also

Table 12

The asymmetric unit of the magnetic structure of α -Mn (#1.85; Lawson *et al.*, 1994) as an example of a structure determined including only constraints forced by the MSG with split sites refined independently.

The approximate relations of the magnetic moments at different sites, if fulfilled exactly, cannot be justified by any increase in the symmetry or any additional irrep restriction, as the symmetry is maximal and only one irrep is active.

α -Mn (#1.85), $I\bar{4}3m1' \rightarrow P_I\bar{4}2_1c$ ($\mathbf{b}_p, \mathbf{a}_p, -\mathbf{c}_p; 0, 0, 0$)

Label	x	y	z	Constraints†	M_x	M_y	M_z	$ \mathbf{M} $
Mn1	0.00000	0.00000	0.00000	$0, 0, m_z$	0.0	0.0	2.83 (13)	2.83
Mn2	0.3192 (2)	0.3192	0.3173 (3)	m_x, m_x, m_z	0.14 (12)	0.14	1.82 (6)	1.83
Mn3_1	0.3621 (1)	0.3621	0.0408 (2)	m_x, m_x, m_z	0.43 (8)	0.43	0.43 (8)	0.74
Mn3_2	0.3533 (2)	0.0333 (1)	0.3559 (2)	m_x, m_y, m_z	-0.25 (10)	-0.25 (10)	-0.32 (4)	0.48
Mn4_1	0.0921 (2)	0.0921	0.2790 (3)	m_x, m_x, m_z	0.27 (8)	0.27	-0.45 (8)	0.59
Mn4_2	0.0895 (2)	0.2850 (1)	0.0894 (2)	m_x, m_y, m_z	-0.08 (4)	-0.45 (8)	0.48 (5)	0.66

† Symmetry constraints on \mathbf{M} .

includes many examples where they have been refined independently.

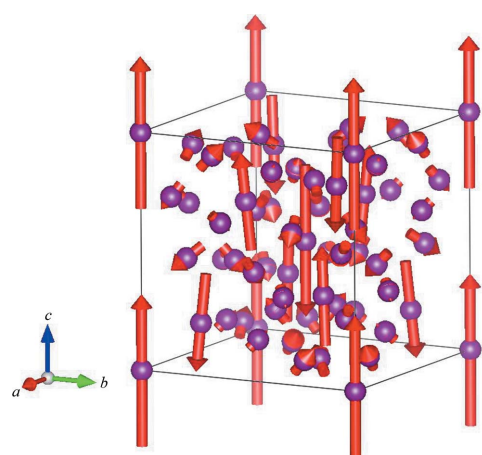
A more subtle simplifying constraint is the assumption of equal moment modulus at magnetic sites which are symmetry independent in the magnetic phase but come from the splitting of a single orbit in the paramagnetic phase. Traditionally, it has been assumed that, if the propagation vector \mathbf{k} is not equivalent to $-\mathbf{k}$, sites related by operations that transform \mathbf{k} into $-\mathbf{k}$ become symmetry split in the magnetic phase. This is not correct in general, as these operations may be maintained within the irrep epikernels. In such cases these sites are kept symmetry related, and therefore the assumption of equal moduli for their magnetic moments is one of the MSG constraints of the phase. In other cases, however, the MSG produces a genuine splitting of the atomic sites, and the assumption of keeping correlated spins is not justified by symmetry arguments. Most of the structures that have genuine split magnetic sites include this simplifying constraint and their spins are assumed to have equal modulus. Table 12 and Fig. 20 summarize the magnetic structure of α -Mn (#1.85; Lawson *et al.*, 1994). This is one of the few examples in the collection where this assumption was not introduced and the

refinement was done fully consistent with the active irrep and relevant MSG, with split sites having independent magnetic moment values.

7. Conclusions

We have gathered a digital collection of more than 400 published magnetic structures under the name *MAGNDATA*, where magnetic symmetry is applied as a robust unambiguous common framework for their description, and a preliminary version is used of the so-called magCIF format, which extends the CIF format to magnetic structures. No validation check has been applied to the structures, and inclusion in the collection has only been subject to the requirement that the published model is self-consistent and unambiguous. The collection is freely available at the Bilbao Crystallographic Server (<http://www.cryst.ehu.es>) and is intended to be a benchmark for a future complete database. This article presents and explains the information that can be retrieved for any of the more than 370 collected commensurate magnetic structures. The various tools that are available for visualization and analysis of each entry have been explained using multiple examples. We have also included a detailed survey of the properties of the collected structures, which shows the power and efficiency of the employed symmetry classification. A subsequent article (Gallego *et al.*, 2016) deals with the more than 40 incommensurate structures that are also included in this collection, using magnetic superspace symmetry as the framework for their description.

We do not have the means to extend *MAGNDATA* to cover all magnetic structures published in the past, or to maintain it and update it regularly for all those published in the future, and therefore this collection does not pretend to become the necessary complete database of all published magnetic structures. However, we hope that this work will stimulate further efforts within the community in the direction of the standardization and unambiguous communication of magnetic structures, with the aim of making such a database possible in the foreseeable future. Meanwhile, authors who have reported a magnetic structure that is absent from this collection and who are interested in having it included are invited to contact us through the given email address.

**Figure 20**

The magnetic structure of α -Mn (#1.85; Lawson *et al.*, 1994), one of the few structures in *MAGNDATA* with a considerable number of independent magnetic sites (some of them symmetry-split by the magnetic order) and which does not include simplifying constraints.

Finally, it should be stressed again that the description of many of the structures within a common framework, with full application of their symmetry properties, has in many cases required a complete transformation and reinterpretation of the information provided by the original references. This may have led to errors and misinterpretations. We therefore welcome and will greatly appreciate any report that may point out such problems.

Acknowledgements

The authors thank Branton Campbell and Harold Stokes for very helpful and fruitful interactions. Their programs *ISODISTORT* and *ISOCIF* were some of the basic tools employed during the realization of this work. We are also indebted to V. Petříček for introducing the magCIF format into the communication tools of his program *JANA*. Very helpful comments and suggestions from Juan Rodriguez-Carvajal are also gratefully acknowledged. One of us (JMPM) is especially indebted to J. L. Ribeiro for helpful comments and interchange of information in the early stages of this work, and to W. Sikora for making available the valuable compilation of magnetic structures done in her group in 1976 and 1984. We also acknowledge the work of student Nagore Garcia, and of her supervisor Irene Urcelay-Olabarria, who gathered and reinterpreted some magnetic structures for this collection. The help of D. Khalyavin and V. Pomjakushin for the introduction of some of their published structures into the database is also gratefully appreciated. This work was supported by the Spanish Ministry of Economy and Competitiveness and FEDER funds (project No. MAT2012-34740/MAT2015-66441-P) and by the Government of the Basque Country (project No. IT779-13).

References

- Aroyo, M. I., Orobengoa, D., de la Flor, G., Tasci, E. S., Perez-Mato, J. M. & Wondratschek, H. (2014). *Acta Cryst. A* **70**, 126–137.
- Ascher, E. (1977). *J. Phys. C Solid State Phys.* **10**, 1365–1377.
- Avdeev, M., Kennedy, B. J. & Kolodiaznyi, T. (2014). *J. Phys. Condens. Matter*, **26**, 095401.
- Avdeev, M., Mohamed, Z., Ling, C. D., Lu, J., Tamaru, M., Yamada, A. & Barpanda, P. (2013). *Inorg. Chem.* **52**, 8685–8693.
- Baran, S., Hofmann, M., Lampert, G., Stüsser, N., Szytuła, A., Többens, D., Smeibidl, P. & Kausche, S. (2001). *J. Magn. Magn. Mater.* **236**, 293–301.
- Baran, S., Kaczorowski, D., Arulraj, A., Penc, B. & Szytuła, A. (2009). *J. Magn. Magn. Mater.* **321**, 3256–3261.
- Belov, N. V., Neronova, N. N. & Smirnova, T. S. (1957). *Sov. Phys. Crystallogr.* **2**, 311–322.
- Bertaut, E. F. (1968). *Acta Cryst. A* **24**, 217–231.
- Bertaut, E. F., Cohen, J., Lambert-Andron, B. & Mollard, P. (1968). *J. Phys. Fr.* **29**, 813–824.
- Bilbao Crystallographic Server (2013). *MGENPOS: General Positions of Magnetic Space Groups and MWYCKPOS: Wyckoff Positions of Magnetic Space Groups*. <http://www.cryst.ehu.es>.
- Blake, G. R., Chapon, L. C., Radaelli, P. G., Park, S., Hur, N., Cheong, S. W. & Rodríguez-Carvajal, J. (2005). *Phys. Rev. B*, **71**, 214402.
- Bradley, C. J. & Cracknell, A. P. (1972). *The Mathematical Theory of Symmetry in Solids*. Oxford: Clarendon Press.
- Brown, P. J. & Chatterji, T. (2006). *J. Phys. Condens. Matter*, **18**, 10085–10096.
- Brown, P. J. & Chatterji, T. (2011). *Phys. Rev. B*, **84**, 054426.
- Brown, P. J. & Forsyth, J. B. (1967). *Proc. Phys. Soc.* **92**, 125–135.
- Brown, P. J. & Forsyth, J. B. (1981). *J. Phys. C Solid State Phys.* **14**, 5171–5184.
- Brown, P. J., Forsyth, J. B., Lelièvre-Berna, E. & Tasset, F. (2002). *J. Phys. Condens. Matter*, **14**, 1957–1966.
- Brown, I. D. & McMahon, B. (2002). *Acta Cryst. B* **58**, 317–324.
- Brown, P. J., Welford, P. J. & Forsyth, J. B. (1973). *J. Phys. C Solid State Phys.* **6**, 1405–1421.
- Buisson, G. (1970). *J. Phys. Chem. Solids*, **31**, 1171–1183.
- Burlet, P., Bourdarot, F., Rossat-Mignod, J., Sanchez, J. P., Spirlet, J. C., Rebizant, J. & Vogt, O. (1992). *Phys. B Condens. Matter*, **180–181**, 131–132.
- Burlet, P., Ressouche, E., Malaman, B., Welter, R., Sanchez, J. P. & Vulliet, P. (1997). *Phys. Rev. B*, **56**, 14013–14018.
- Calder, S., Lumsden, M. D., Garlea, V. O., Kim, J. W., Shi, Y. G., Feng, H. L., Yamaura, K. & Christianson, A. D. (2012). *Phys. Rev. B*, **86**, 054403.
- Calder, S., Saparov, B., Cao, H. B., Niedziela, J. L., Lumsden, M. D., Sefat, A. S. & Christianson, A. D. (2014). *Phys. Rev. B*, **89**, 064417.
- Campbell, B. J., Stokes, H. T., Tanner, D. E. & Hatch, D. M. (2006). *J. Appl. Cryst.* **39**, 607–614.
- Caron, J. M., Neilson, J. R., Miller, D. C., Llobet, A. & McQueen, T. M. (2011). *Phys. Rev. B*, **84**, 180409.
- Chattopadhyay, T., Brown, P. J., Roessli, B., Stepanov, A. A., Barilo, S. N. & Zhigunov, D. I. (1992). *Phys. Rev. B*, **46**, 5731–5734.
- Christianson, A. D., Lumsden, M. D., Angst, M., Yamani, Z., Tian, W., Jin, R., Payzant, E. A., Nagler, S. E., Sales, B. C. & Mandrus, D. (2008). *Phys. Rev. Lett.* **100**, 107601.
- Corliss, L. M., Elliott, N. & Hastings, J. M. (1960). *Phys. Rev.* **117**, 929–935.
- Damay, F., Martin, C., Hardy, V., André, G., Petit, S. & Maignan, A. (2011). *Phys. Rev. B*, **83**, 184413.
- Damay, F., Poienaru, M., Martin, C., Maignan, A., Rodriguez-Carvajal, J., André, G. & Doumerc, J. P. (2009). *Phys. Rev. B*, **80**, 094410.
- Deldem, M., Amara, M., Galéra, R. M., Morin, P., Schmitt, D. & Ouladdiaf, B. (1998). *J. Phys. Condens. Matter*, **10**, 165–174.
- Ding, L., Colin, C. V., Darie, C., Robert, J., Gay, F. & Bordet, P. (2016). *Phys. Rev. B*, **93**, 064423.
- Dul, M., Lesniewska, B., Oles, A., Pytlak, L. & Sikora, W. (1997). *Phys. B Condens. Matter*, **234–236**, 790–791.
- Ederer, C. & Spaldin, N. A. (2007). *Phys. Rev. B*, **76**, 214404.
- Ehrenberg, H., Witschek, G., Rodriguez-Carvajal, J. & Vogt, T. (1998). *J. Magn. Magn. Mater.* **184**, 111–115.
- Fernández-Díaz, M. T., Martínez, J. L., Alonso, J. M. & Herrero, E. (1999). *Phys. Rev. B*, **59**, 1277–1284.
- Fiebig, M., Fröhlich, D. & Thiele, H. J. (1996). *Phys. Rev. B*, **54**, R12681–R12684.
- Free, D. G. & Evans, J. S. (2010). *Phys. Rev. B*, **81**, 214433.
- Fruchart, D. & Bertaut, E. F. (1978). *J. Phys. Soc. Jpn.* **44**, 781–791.
- Fruchart, D., Bertaut, E. F., Sayetat, F., Nasr Eddine, M., Fruchart, R. & Séanteur, J. P. (1970). *Solid State Commun.* **8**, 91–99.
- Gäbler, F., Schnelle, W., Senyshyn, A. & Niewa, R. (2008). *Solid State Sci.* **10**, 1910–1915.
- Gallego, S. V., Perez-Mato, J. M., Elcoro, L., Tasci, E. S., Hanson, R. L., Aroyo, M. I. & Madariaga, G. (2016). *J. Appl. Cryst.* **49**, doi:10.1107/S1600576716015491.
- Gallego, S. V., Tasci, E. S., de la Flor, G., Perez-Mato, J. M. & Aroyo, M. I. (2012). *J. Appl. Cryst.* **45**, 1236–1247.
- Glazer, A. M., Aroyo, M. I. & Authier, A. (2014). *Acta Cryst. A* **70**, 300–302.
- Goldman, A. I., Argyriou, D. N., Ouladdiaf, B., Chatterji, T., Kreyssig, A., Nandi, S., Ni, N., Bud'ko, S. L., Canfield, P. C. & McQueeney, R. J. (2008). *Phys. Rev. B*, **78**, 100506.
- Gorbunov, D. I., Henriques, M. S., Andreev, A. V., Eigner, V., Gukasov, A., Fabrèges, X., Skourski, Y., Petříček, V. & Wosnitza, J. (2016). *Phys. Rev. B*, **93**, 024407.

- Hahn, Th. (2002). (Editor). *International Tables for Crystallography*, Vol. A, *Space-Group Symmetry*, 5th ed. Dordrecht: Kluwer Academic Publishers.
- Hamasaki, T., Ide, T., Kuroe, H., Sekine, T., Hase, M., Tsukada, I. & Sakakibara, T. (2008). *Phys. Rev. B*, **77**, 134419.
- Hanson, R. (2013). *Jmol: An Open-Source Java Viewer for Chemical Structures in Three Dimensions*. <http://www.jmol.org/>.
- Hase, M., Kuroe, H., Pomjakushin, V. Y., Keller, L., Tamura, R., Terada, N., Matsushita, Y., Dönni, A. & Sekine, T. (2015). *Phys. Rev. B*, **92**, 054425.
- Hastings, J. M., Corliss, L. M. & Windsor, C. G. (1965). *Phys. Rev.* **138**, A176–A177.
- Hill, A. H., Jiao, F., Bruce, P. G., Harrison, A., Kockelmann, W. & Ritter, C. (2008). *Chem. Mater.* **20**, 4891–4899.
- Huang, Q., Qiu, Y., Bao, W., Green, M. A., Lynn, J. W., Gasparovic, Y. C., Wu, T., Wu, G. & Chen, X. H. (2008). *Phys. Rev. Lett.* **101**, 257003.
- Hutana, V., Sazonov, A., Meven, M., Murakawa, H., Tokura, Y., Bordács, S., Kézsmárki, I. & Náfrádi, B. (2012). *Phys. Rev. B*, **86**, 104401.
- Hwang, J., Choi, E. S., Ye, F., Dela Cruz, C. R., Xin, Y., Zhou, H. D. & Schlottmann, P. (2012). *Phys. Rev. Lett.* **109**, 257205.
- ICSD (2007). Inorganic Crystal Structure Database. FIZ-Karlsruhe, Germany, and the National Institute of Standards and Technology, USA. <http://www.fiz-karlsruhe.de/icsd.html>.
- Iikubo, S., Kodama, K., Takenaka, K., Takagi, H. & Shamoto, S. (2008). *Phys. Rev. B*, **77**, 020409.
- International Union of Crystallography (2015). *Commission on Magnetic Structures*. <http://www.iucr.org/iucr/commissions/magnetic-structures>.
- Ivanov, S. A., Tellgren, R., Ritter, C., Nordblad, P., Mathieu, R., André, G., Golubko, N. V., Politova, E. D. & Weil, M. (2012). *Mater. Res. Bull.* **47**, 63–72.
- Izyumov, Y. A., Naish, V. E. & Ozerov, R. P. (1991). *Neutron Diffraction of Magnetic Materials*. Dordrecht: Kluwer Academic Publishers.
- Jauch, W., Reehuis, M., Bleif, H. J., Kubanek, F. & Pattison, P. (2001). *Phys. Rev. B*, **64**, 052102.
- Jensen, T. B. S., Christensen, N. B., Kenzelmann, M., Rønnow, H. M., Niedermayer, C., Andersen, N. H., Lefmann, K., Schefer, J., Zimmermann, M., Li, J., Zarestky, J. L. & Vaknin, D. (2009). *Phys. Rev. B*, **79**, 092412.
- Kenzelmann, M., Coldea, R., Tennant, D. A., Visser, D., Hofmann, M., Smeibidl, P. & Tylicki, Z. (2002). *Phys. Rev. B*, **65**, 144432.
- Knížek, K., Jirák, Z., Novák, P. & de la Cruz, C. (2014). *Solid State Sci.* **28**, 26–30.
- Kréen, E., Kádár, G., Pál, L. & Szabó, P. (1967). *J. Appl. Phys.* **38**, 1265–1266.
- Kunnemann, W., La Placa, S., Corliss, L. M., Hastings, J. M. & Banks, E. (1968). *J. Phys. Chem. Solids*, **29**, 1359–1364.
- Law, J. M., Koo, H. J., Whangbo, M. H., Brücher, E., Pomjakushin, V. & Kremer, R. K. (2014). *Phys. Rev. B*, **89**, 014423.
- Lawson, A. C., Larson, A. C., Aronson, M. C., Johnson, S., Fisk, Z., Canfield, P. C., Thompson, J. D. & Von Dreele, R. B. (1994). *J. Appl. Phys.* **76**, 7049–7051.
- Lefrançois, E., Chapon, L. C., Simonet, V., Lejay, P., Khalyavin, D., Rayaprol, S., Sampathkumaran, E. V., Ballou, R. & Adroja, D. T. (2014). *Phys. Rev. B*, **90**, 014408.
- Litvin, D. B. (2013). *Magnetic Group Tables: 1-, 2- and 3-Dimensional Magnetic Subperiodic Groups and Magnetic Space Groups*. Chester: International Union of Crystallography. <http://www.iucr.org/publ/978-0-9553602-2-0>.
- López, M. L., Daidouh, A., Pico, C., Rodríguez-Carvajal, J. & Veiga, M. L. (2008). *Chem. Eur. J.* **14**, 10829–10838.
- Lovesey, S. W., Khalyavin, D. D., Manuel, P., Chapon, L. C., Cao, G. & Qi, T. F. (2012). *J. Phys. Condens. Matter*, **24**, 496003.
- Martinelli, A., Ferretti, M. & Ritter, C. (2016). *J. Solid State Chem.* **239**, 99–105.
- Martínez-Coronado, R., Alonso, J. A., Cascos, V. & Fernández-Díaz, M. T. (2014). *J. Power Sources*, **247**, 876–882.
- Matsuda, M., de la Cruz, C., Yoshida, H., Isobe, M. & Fishman, R. S. (2012). *Phys. Rev. B*, **85**, 144407.
- Melot, B. C., Padén, B., Seshadri, R., Suard, E., Néner, G., Dixit, A. & Lawes, G. (2010). *Phys. Rev. B*, **82**, 014411.
- Momma, K. & Izumi, F. (2011). *J. Appl. Cryst.* **44**, 1272–1276.
- Müller, H., Kockelmann, W. & Johrendt, D. (2006). *Chem. Mater.* **18**, 2174–2180.
- Müller, R. A., Lee-Hone, N. R., Lapointe, L., Ryan, D. H., Pereg-Barnea, T., Bianchi, A. D., Mozharivskyj, Y. & Flacau, R. (2014). *Phys. Rev. B*, **90**, 041109.
- Muñoz, A., Alonso, J. A., Casais, M. T., Martínez-Lope, M. J., Martínez, J. L. & Fernández-Díaz, M. T. (2002). *Phys. Rev. B*, **65**, 144423.
- Muñoz, A., Alonso, J. A., Martínez-Lope, M. J., Casáis, M. T., Martínez, J. L. & Fernández-Díaz, M. T. (2000). *Phys. Rev. B*, **62**, 9498–9510.
- Muñoz, A., Alonso, J. A., Martínez-Lope, M. J., Casáis, M. T., Martínez, J. L. & Fernández-Díaz, M. T. (2001). *Chem. Mater.* **13**, 1497–1505.
- Muñoz, A., Casáis, M. T., Alonso, J. A., Martínez-Lope, M. J., Martínez, J. L. & Fernández-Díaz, M. T. (2001). *Inorg. Chem.* **40**, 1020–1028.
- Murakawa, H., Onose, Y., Miyahara, S., Furukawa, N. & Tokura, Y. (2010). *Phys. Rev. Lett.* **105**, 137202.
- Núñez, P., Roisnel, T. & Tressaud, A. (1994). *Solid State Commun.* **92**, 601–605.
- Oles, A., Kajzar, P., Kucab, M. & Sikora, W. (1976). *Magnetic Structures Determined by Neutron Diffraction*. Warszawa, Krakow: Państwowe Wydawnictwo Naukowe.
- Oles, A., Sikora, W., Bombik, A. & Konopka, M. (1984). *Magnetic Structure Determined by Neutron Diffraction. Description and Symmetry Analysis*. Scientific Bulletins of the Stanisław Staszic University of Mining and Metallurgy, No. 1005. Krakow.
- Opechowski, W. & Guccione, R. (1965). *Magnetism*, edited by G. T. Rado & H. Suhl, Vol. II, Part A, pp. 105–165. New York: Academic Press.
- Perez-Mato, J. M., Gallego, S. V., Elcoro, L., Tasci, E. S. & Aroyo, M. I. (2016). *J. Phys. Condens. Matter*, **28**, 286001.
- Perez-Mato, J. M., Gallego, S. V., Tasci, E. S., Elcoro, L., de la Flor, G. & Aroyo, M. I. (2015). *Annu. Rev. Mater. Res.* **45**, 217–248.
- Perez-Mato, J. M. & Ribeiro, J. L. (2011). *Acta Cryst. A* **67**, 264–268.
- Perez-Mato, J. M., Ribeiro, J. L., Petříček, V. & Aroyo, M. I. (2012). *J. Phys. Condens. Matter*, **24**, 163201.
- Pernet, M., Elmalek, D. & Joubert, J. C. (1970). *Solid State Commun.* **8**, 1583–1587.
- Petříček, V., Dušek, M. & Palatinus, L. (2014). *Z. Kristallogr.* **229**, 345–352.
- Petříček, V., Fuksa, J. & Dušek, M. (2010). *Acta Cryst. A* **66**, 649–655.
- Plumier, R., Sougi, M. & Saint-James, R. (1983). *Phys. Rev. B*, **28**, 4016–4020.
- Pomjakushin, V. Y., Pomjakushina, E. V., Krzton-Maziopa, A., Conder, K. & Shermadini, Z. (2011). *J. Phys. Condens. Matter*, **23**, 156003.
- Poole, A., Wills, A. S. & Lelièvre-Berna, E. (2007). *J. Phys. Condens. Matter*, **19**, 452201.
- Radaelli, P. G., Cox, D. E., Capogna, L., Cheong, S. W. & Marezio, M. (1999). *Phys. Rev. B*, **59**, 14440–14450.
- Ratcliff, W. II, Lima Sharma, A. L., Gomes, A. M., Gonzalez, J. L., Huang, Q. & Singleton, J. (2009). *J. Magn. Magn. Mater.* **321**, 2612–2616.
- Redhammer, G. J., Roth, G., Treutmann, W., Hoelzel, M., Paulus, W., André, G., Pietzonka, C. & Amthauer, G. (2009). *J. Solid State Chem.* **182**, 2374–2384.
- Redhammer, G. J., Roth, G., Treutmann, W., Paulus, W., André, G., Pietzonka, C. & Amthauer, G. (2008). *J. Solid State Chem.* **181**, 3163–3176.

- Reehuis, M., Ulrich, C., Prokeš, K., Mat'aš, S., Fujioka, J., Miyasaka, S., Tokura, Y. & Keimer, B. (2011). *Phys. Rev. B*, **83**, 064404.
- Ressouche, E., Kernavanois, N., Regnault, L. P. & Henry, J. Y. (2006). *Phys. B Condens. Matter*, **385–386**, 394–397.
- Ressouche, E., Loire, M., Simonet, V., Ballou, R., Stunault, A. & Wildes, A. (2010). *Phys. Rev. B*, **82**, 100408.
- Rodríguez, E. E., Cao, H., Haiges, R. & Melot, B. C. (2016). *J. Solid State Chem.* **236**, 39–44.
- Rodríguez-Carvajal, J. (1993). *Phys. B Condens. Matter*, **192**, 55–69.
- Rousse, G., Rodriguez-Carvajal, J., Patoux, S. & Masquelier, C. (2003). *Chem. Mater.* **15**, 4082–4090.
- Saha, R., Sundaresan, A., Sanyal, M. K., Rao, C. N. R., Orlandi, F., Manuel, P. & Langridge, S. (2016). *Phys. Rev. B*, **93**, 014409.
- Sazonov, A. P., Gukasov, A., Cao, H. B., Bonville, P., Ressouche, E., Decorse, C. & Mirebeau, I. (2013). *Phys. Rev. B*, **88**, 184428.
- Scagnoli, V., Allieta, M., Walker, H., Scavini, M., Katsufuji, T., Sagarna, L., Zaharko, O. & Mazzoli, C. (2012). *Phys. Rev. B*, **86**, 094432.
- Schmid, H. (2001). *Ferroelectrics*, **252**, 41–50.
- Schobinger-Papamantellos, P., Buschow, K. H. J. & Rodríguez-Carvajal, J. (2012). *J. Magn. Magn. Mater.* **324**, 3709–3715.
- Schobinger-Papamantellos, P., De Mooij, D. B. & Buschow, K. H. J. (1988). *J. Less-Common Met.* **144**, 265–274.
- Schobinger-Papamantellos, P., Rodríguez-Carvajal, J., André, G. & Buschow, K. H. J. (2006). *J. Magn. Magn. Mater.* **300**, 333–350.
- Schobinger-Papamantellos, P., Rodríguez-Carvajal, J., André, G., Duong, N. P., Buschow, K. H. J. & Tolédano, P. (2001). *J. Magn. Magn. Mater.* **236**, 14–27.
- Shirane, G. J., Pickart, S. & Ishikawa, Y. (1959). *J. Phys. Soc. Jpn.* **14**, 1352–1360.
- Shull, C. G. & Smart, J. S. (1949). *Phys. Rev.* **76**, 1256–1257.
- Spaldin, N. A., Fiebig, M. & Mostovoy, M. (2008). *J. Phys. Condens. Matter*, **20**, 434203.
- Stokes, H. T. & Campbell, B. J. (2011). *ISO-Mag: Table of Magnetic Space Groups. ISOTROPY Software Suite*. <http://iso.byu.edu>.
- Stokes, H. T. & Campbell, B. J. (2015). *ISOCIF: Create or Modify CIF files. ISOTROPY Software Suite*. <http://iso.byu.edu>.
- Stokes, H. T., Campbell, B. J. & Cordes, R. (2013). *Acta Cryst. A* **69**, 388–395.
- Szytuła, A., Baran, S., Kaczorowski, D., Sikora, W. & Hoser, A. (2014). *J. Alloys Compd.* **617**, 149–153.
- Taira, N., Wakushima, M., Hinatsu, Y., Tobo, A. & Ohoyama, K. (2003). *J. Solid State Chem.* **176**, 165–169.
- Tan, L., Kreyssig, A., Kim, J. W., Goldman, A. I., McQueeney, R. J., Wermeille, D., Sieve, B., Lograsso, T. A., Schlagel, D. L., Budko, S. L., Pecharsky, V. K. & Gschneidner, K. A. (2005). *Phys. Rev. B*, **71**, 214408.
- Toft-Petersen, R., Reehuis, M., Jensen, T. B., Andersen, N. H., Li, J., Le, M. D., Laver, M., Niedermayer, C., Klemke, B., Lefmann, K. & Vaknin, D. (2015). *Phys. Rev. B*, **92**, 024404.
- Troć, R., Pasturel, M., Tougait, O., Sazonov, A. P., Gukasov, A., Sulkowski, C. & Noël, H. (2012). *Phys. Rev. B*, **85**, 064412.
- Tsuzuki, K., Ishikawa, Y., Watanabe, N. & Akimoto, S. (1974). *J. Phys. Soc. Jpn.* **37**, 1242–1247.
- Vecchini, C., Chapon, L. C., Brown, P. J., Chatterji, T., Park, S., Cheong, S. W. & Radaelli, P. G. (2008). *Phys. Rev. B*, **77**, 134434.
- Vilminot, S., André, G. & Kurmoo, M. (2009). *Inorg. Chem.* **48**, 2687–2692.
- Wheeler, E. M., Lake, B., Islam, A. N., Reehuis, M., Steffens, P., Guidi, T. & Hill, A. H. (2010). *Phys. Rev. B*, **82**, 140406.
- Wiebe, C. R., Gardner, J. S., Kim, S. J., Luke, G. M., Wills, A. S., Gaulin, B. D., Greedan, J. E., Swainson, I., Qiu, Y. & Jones, C. Y. (2004). *Phys. Rev. Lett.* **93**, 076403.
- Will, G. & Schafer, W. (1979). *J. Less-Common Met.* **67**, 31–39.
- Wills, A. S., Zhitomirsky, M. E., Canals, B., Sanchez, J. P., Bonville, P., de Réotier, P. D. & Yaouanc, A. (2006). *J. Phys. Condens. Matter*, **18**, L37–L42.
- Yamaura, J., Ohgushi, K., Ohsumi, H., Hasegawa, T., Yamauchi, I., Sugimoto, K., Takeshita, S., Tokuda, A., Takata, M., Udagawa, M., Takigawa, M., Harima, H., Arima, T. & Hiroi, Z. (2012). *Phys. Rev. Lett.* **108**, 247205.
- Yan, B., Paul, A. K., Kanungo, S., Reehuis, M., Hoser, A., Többens, D. M., Schnelle, W., Williams, R. C., Lancaster, T., Xiao, F., Möller, J. S., Blundell, S. J., Hayes, W., Felser, C. & Jansen, M. (2014). *Phys. Rev. Lett.* **112**, 147202.
- Yano, S., Louca, D., Yang, J., Chatterjee, U., Bugaris, D. E., Chung, D. Y., Peng, L., Grayson, M. & Kanatzidis, M. G. (2016). *Phys. Rev. B*, **93**, 024409.
- Ye, F., Chi, S., Chakoumakos, B. C., Fernandez-Baca, J. A., Qi, T. & Cao, G. (2013). *Phys. Rev. B*, **87**, 140406.
- Yelon, W. B. & Cox, D. E. (1973). *Phys. Rev. B*, **7**, 2024–2027.
- Zhu, M., Do, D., Dela Cruz, C. R., Dun, Z., Zhou, H. D., Mahanti, S. D. & Ke, X. (2014). *Phys. Rev. Lett.* **113**, 076406.